

# Palladium Complexes with Chiral Diphospholane Ligands: Comparative Catalytic Properties and Analysis of ( $\eta^3$ -Allyl)palladium Species

Grégory Malaisé,<sup>[a]</sup> Shailesh Ramdeehul,<sup>[a]</sup> John A. Osborn,<sup>\*,[a][†]</sup> Laurent Barloy,<sup>\*,[a]</sup> Nathalie Kyritsakas,<sup>[b]</sup> and Roland Graff<sup>[c]</sup>

*Dedicated to the memory of Jean-Marc Kern*

**Keywords:** Palladium / Allyl ligands / Reaction intermediates / Asymmetric catalysis / Enantioselectivity

The chiral diphospholane ligands Duphos (**1**) and Duxantphos (**2**), which can be differentiated by their bite angle, were applied to palladium-catalysed asymmetric reactions, essentially allylic alkylations with symmetrically (**3a–d**) or unsymmetrically (**5a,b**) substituted allylic acetates as substrates. The most interesting results were found with the first series of substrates in which **2** was more reactive and/or selective than **1**. The model complexes of the catalytic intermediates [Pd{(S,S)-**1**}( $\eta^3$ -cyclohexenyl)](BF<sub>4</sub>) (**10**) and exo-[Pd{(R,R)-**2**}( $\eta^3$ -cyclohexenyl)](SbF<sub>6</sub>) (**11**) could be characterised by X-ray crystallography. <sup>1</sup>H and <sup>31</sup>P NMR spectroscopic analyses of [Pd{(R,R)-**2**}( $\eta^3$ -diphenylallyl)](SbF<sub>6</sub>) (**12**)

and [Pd{(R,R)-**2**}( $\eta^3$ -allyl)](SbF<sub>6</sub>) (**13**) revealed the presence of exchanging isomers in solution. Structural data provided by these techniques combined with the preferential rotation model led to a satisfactory interpretation of the catalytic allylic alkylation results. It appears that the bite angle plays a crucial role in the positioning of the proximal methyl groups, which determines the distribution of allyl isomeric intermediates and the balance between clockwise and anticlockwise rotations in the enantioselective step.

(© Wiley-VCH Verlag GmbH & Co. KGaA, 69451 Weinheim, Germany, 2004)

## Introduction

Asymmetric palladium-catalysed reactions have attracted enormous interest over the past years, especially for allylic substitutions<sup>[1,2a]</sup> or the Heck reaction.<sup>[2b]</sup> Allylic alkylation is of considerable use in organic synthesis and proceeds smoothly under mild conditions. A large amount of work has been devoted to the design and synthesis of chiral ligands, with the aim of increasing the enantioselectivity of the catalysts. Very good asymmetric inductions have been achieved, most of them with the benchmark substrate 1-acetoxy-1,3-diphenylprop-2-ene, but also with sterically less demanding substrates such as 1-acetoxycyclohex-2-ene.<sup>[1,2a]</sup> Structural analyses of allyl palladium intermediates have

been helpful in understanding the intimate steric and/or electronic grounds for enantioselectivity.<sup>[1a–1c,2a,3]</sup>

The catalytic properties of two chiral xanthene-derived ligands for use in allylic alkylations have been previously reported in the laboratory.<sup>[4]</sup> These ligands combine the advantages of having chiral phospholane donor groups, which have met with great success in catalysis,<sup>[5]</sup> and a wide bite angle. The advantages of large bite angle ligands in homogeneous catalysis are well known<sup>[6]</sup> and, furthermore, an increase of the P–Pd–P angle imposed by the ligand is likely to improve the control of allylic alkylation enantioselectivity through enhancement of the depth of the chiral pocket.<sup>[1b]</sup>

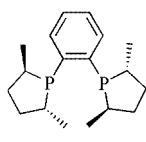
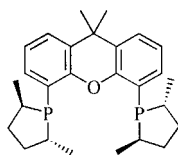
The purpose of this paper is to report a systematic comparison between one of these ligands, 4,5-bis[(2*R*,5*R*)-2,5-dimethylphospholanyl]-9,9-dimethylxanthene, hereafter abbreviated (*R,R*)-Duxantphos [(*R,R*)-**2**], with the homologous bidentate, narrow bite angle ligand (*R,R*)-Duphos<sup>[5]</sup> [(*R,R*)-**1**] or its enantiomer (*S,S*)-**1**. This comparison relates to their application in palladium-catalysed asymmetric reactions and to the three-dimensional structural properties of their respective allyl palladium(II) complexes in order to rationalise their catalytic behaviour.

<sup>[a]</sup> Laboratoire de Chimie des Métaux de Transition et de Catalyse, UMR 7513 CNRS, Institut Le Bel, Université Louis Pasteur, 4 rue Blaise Pascal, 67070 Strasbourg Cedex, France  
Fax: (internat.) + 33-3-90241329  
E-mail: barloy@chimie.u-strasbg.fr

<sup>[b]</sup> Service commun des Rayons X, Faculté de Chimie, Institut Le Bel, Université Louis Pasteur, 4 rue Blaise Pascal, 67070 Strasbourg Cedex, France

<sup>[c]</sup> Service commun de RMN, Faculté de Chimie, Université Louis Pasteur, 1 rue Blaise Pascal, 67008 Strasbourg Cedex, France

<sup>[†]</sup> Deceased; please address further correspondence to L. Barloy

(R,R)-Duphos  
(R,R)-1(R,R)-Duxantphos  
(R,R)-2

## Results

### Homogeneous Catalysis

The ligands Duphos (**1**) and Duxantphos (**2**) were first tested in palladium-catalysed allylic alkylation with the racemic allylic acetates **3**–**6** as substrates, the standard dimethyl malonate anion as the nucleophile and  $[\text{Pd}(\text{C}_3\text{H}_5)\text{Cl}]_2$  as the palladium source. The results are shown in Table 1. All tests were run using ligands with the (*R,R*) configuration, except one (Entry 11). The nucleophile was generated from dimethyl malonate either using sodium hydride, or in situ with *N,O*-bis(trimethylsilyl)acetamide (BSA) and a catalytic amount of sodium acetate.

These results show interesting differences between **1** and **2** with regard to reactivity and selectivity. In general, the Pd catalyst is less reactive with ligand **1** than with ligand **2**. BSA does not appear to be an appropriate base for **1** (Entries 6, 9, 11), leading at best to low yields (0–30%). Quantitative yields are obtained only with NaH. On the contrary, the catalytic alkylation reactions are complete with ligand **2** whatever the base, solvent or temperature. Furthermore, with the cyclic substrates 1-acetoxycyclohex-2-ene (**3c**) or 1-acetoxycyclopent-2-ene (**3d**), the reactions are finished

within very short time ranges (5–10 min, see Entries 10, 12–14).

With 1-acetoxy-1,3-diphenylprop-2-ene (**3a**) as substrate, both ligands give rise to high *ee* values which is also the case for a host of chiral ligands reported in the literature.<sup>[1]</sup> Under the same conditions, ligand **1** leads to a 97% *ee* in 4 h, whereas ligand **2** affords a faster reaction (1 h) but with a lower enantioselectivity (85% *ee*) (Entries 1 and 2). Although the configurations of **1** and **2** are the same [viz (*R,R*)], the configurations of the major enantiomer of product **4a** are the opposite. The *ee* value found for **1** is practically identical to that reported by Pregosin et al. (98%) for the same reaction run with (*R,R*)-**1** but with conditions slightly different from ours (BSA/ $\text{CH}_2\text{Cl}_2$ ).<sup>[7]</sup> With ligand **2**, the *ee* could be increased to up to 97% by modifying the base and solvent and to a higher extent by lowering the temperature (Entries 3 and 4).

The difference between both diphospholane ligands with regards to enantio-differentiation is far more striking with the sterically less demanding substrates **3b–d**, with a marked superiority of **2** over **1**. Low enantiomeric excesses were observed using ligand **1** (5–10%, Entries 5, 8, 11). In contrast, ligand **2** affords high *ee* values with 2-acetoxypent-3-ene (**3b**) and 1-acetoxycyclohex-2-ene (**3c**) (75%, Entry 7 and 83%, Entry 10, respectively). The performance of ligand (*R,R*)-**2** in terms of enantioselectivity is similar to that previously reported under somewhat different reaction conditions.<sup>[4]</sup> The asymmetric induction is, however, less efficient (50–54% *ee*) when one switches to the cyclopentenyl substrate **3d** (Entries 12–14) but **2** still remains superior to **1**. Incidentally, the configurations of the major enantiomers of **4c** and **4d** are the same (*S*) with ligand **2**.

Table 1. Palladium-catalysed asymmetric allylic alkylations of racemic allylic acetates **3a–d** with dimethyl malonate using diphospholane ligands **1** and **2**

Entry	Substrate	Ligand	Base	Solvent	Temperature	Time <sup>[a]</sup>	<i>ee</i> [%] <sup>[b]</sup>
1	<b>3a</b>	( <i>R,R</i> )- <b>1</b>	NaH	THF	room temp.	4 h	97 ( <i>S</i> )
2	<b>3a</b>	( <i>R,R</i> )- <b>2</b>	NaH	THF	room temp.	1 h	85 ( <i>R</i> )
3	<b>3a</b>	( <i>R,R</i> )- <b>2</b>	BSA/KOAc	$\text{CH}_2\text{Cl}_2$	room temp.	1 h	89 ( <i>R</i> )
4	<b>3a</b>	( <i>R,R</i> )- <b>2</b>	BSA/KOAc	$\text{CH}_2\text{Cl}_2$	0 °C	3 h	97 ( <i>R</i> )
5	<b>3b</b>	( <i>R,R</i> )- <b>1</b>	NaH	THF	room temp.	4 h	9 ( <i>R</i> )
6	<b>3b</b>	( <i>R,R</i> )- <b>1</b>	BSA/KOAc	$\text{CH}_2\text{Cl}_2$	room temp.	24 h	– <sup>[c]</sup>
7	<b>3b</b>	( <i>R,R</i> )- <b>2</b>	BSA/KOAc	$\text{CH}_2\text{Cl}_2$	room temp.	3.5 h	75 ( <i>S</i> )
8	<b>3c</b>	( <i>R,R</i> )- <b>1</b>	NaH	THF	room temp.	3 h	5 ( <i>S</i> )
9	<b>3c</b>	( <i>R,R</i> )- <b>1</b>	BSA/KOAc	$\text{CH}_2\text{Cl}_2$	room temp.	24 h	– <sup>[d]</sup>
10	<b>3c</b>	( <i>R,R</i> )- <b>2</b>	NaH	THF	0 °C	10 min	83 ( <i>S</i> )
11	<b>3d</b>	( <i>S,S</i> )- <b>1</b>	BSA/KOAc	$\text{CH}_2\text{Cl}_2$	room temp.	24 h	10 ( <i>R</i> ) <sup>[e]</sup>
12	<b>3d</b>	( <i>R,R</i> )- <b>2</b>	BSA/KOAc	$\text{CH}_2\text{Cl}_2$	room temp.	10 min	50 ( <i>S</i> )
13	<b>3d</b>	( <i>R,R</i> )- <b>2</b>	BSA/KOAc	THF	room temp.	5 min	52 ( <i>S</i> )
14	<b>3d</b>	( <i>R,R</i> )- <b>2</b>	NaH	THF	0 °C	7 min	54 ( <i>S</i> )

<sup>[a]</sup> The yields determined by GC (using dodecane as internal standard) were quantitative unless otherwise stated. <sup>[b]</sup> See Exp. Sect. The absolute configuration is given in parentheses. <sup>[c]</sup> No reaction. <sup>[d]</sup> 1% yield. <sup>[e]</sup> 30% yield.

Table 2. Palladium-catalysed asymmetric allylic alkylations of racemic allylic acetates **5a–b** with dimethyl malonate using diphospholane ligands **1** and **2**

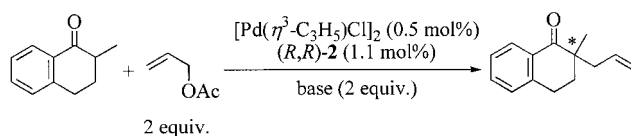
Entry	Substrate	Ligand	Base	Solvent	Time <sup>[a]</sup>	Yield ( <i>ee</i> ) [%] <b>6</b>	Yield ( <i>ee</i> ) [%] <b>7</b>
1	<b>5a</b>	( <i>S,S</i> )- <b>1</b>	BSA/KOAc	CH <sub>2</sub> Cl <sub>2</sub>	24 h	96 (12) <sup>[b]</sup>	4 (80)
2	<b>5a</b>	( <i>R,R</i> )- <b>2</b>	BSA/KOAc	CH <sub>2</sub> Cl <sub>2</sub>	24 h	95 (3) <sup>[c]</sup>	1 (60)
3	<b>5a</b>	( <i>R,R</i> )- <b>2</b>	BSA/KOAc	THF	2 h	98 (16) <sup>[b]</sup>	2 (55)
4	<b>5a</b>	( <i>R,R</i> )- <b>2</b>	NaH	THF	5 min	98 (3) <sup>[b]</sup>	2 (15)
5	<b>5b</b>	( <i>S,S</i> )- <b>1</b>	NaH	THF	24 h	3 (nd) <sup>[d]</sup>	0
6	<b>5b</b>	( <i>R,R</i> )- <b>2</b>	NaH	THF	1 h	90 (0)	0
7	<b>5b</b>	( <i>R,R</i> )- <b>2</b>	BSA/KOAc	THF	24 h	0	0
8	<b>5b</b>	( <i>R,R</i> )- <b>2</b>	BSA/KOAc	CH <sub>2</sub> Cl <sub>2</sub>	24 h	20 (0)	0

<sup>[a]</sup> See Exp. Sect. The reactions were performed at room temperature and the yields determined by GC using dodecane as internal standard. <sup>[b]</sup> (*S*) configuration. <sup>[c]</sup> (*R*) configuration. <sup>[d]</sup> nd = not determined.

We were also interested in the regiochemical and stereochemical outcome of the alkylation by dimethylmalonate of unsymmetrically substituted allylic acetates, viz 2-acetoxy-4-phenylbut-3-ene (**5a**) and 3-acetoxy-2-methylhex-4-ene (**5b**), catalysed by palladium associated with the diphospholane ligands (Table 2). With substrate **5a** the conversion is always complete, but the reaction time strongly depends on the reaction conditions from 5 min (Entry 4) to 24 h (Entry 2). The nucleophile attacks overwhelmingly on the Me side of the allyl intermediate to yield **6a** as the major product, whatever the ligand. This is a general trend with this substrate,<sup>[8–10]</sup> due to delocalization of the C=C bond with the phenyl substituent. The *ee* values of **6a** are poor (3–16%), whereas they are far better for the minor regioisomer **7a** (up to 80%). This situation mirrors the predictions and experimental results reported by Norrby, Åkermærk, Helquist et al. for the same substrate.<sup>[9]</sup> The differences between both ligands **1** and **2** are rather minor. Under the same conditions (BSA/CH<sub>2</sub>Cl<sub>2</sub>), Duphos (**1**) performs slightly better than Duxantphos (**2**) in terms of enantioselectivity (Entries 1 and 2), but the *ee* of **6a** can be improved to 16% with **2** using THF as the solvent (Entry 3). Substrate **5b** appears less reactive and it is necessary to use NaH as a base to achieve a good conversion (90%) with ligand **2**. Under the same conditions, ligand **1** is almost inactive (3% conversion in 24 h, Entry 5). Only one regioisomeric product, **6b**, was formed and no asymmetric induction was observed. Under our conditions, the allyl palladium intermediates derived from (*R*)-**5a,b** do not interconvert with those derived from (*S*)-**5a,b**. A powerful memory effect can therefore be expected which results in poor global *ee* values,<sup>[11]</sup> taking into account that allylic alkylation proceeds with overall retention of configuration and that the regioisomers **6a,b** are the overwhelmingly major catalysis products.<sup>[2a]</sup>

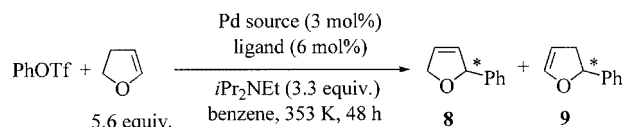
The good performance of ligand (*R,R*)-**2** with small substrates (*vide supra*) prompted us to carry out the alkylation

of the simple allyl acetate (2 equiv.) with the prochiral nucleophile (1 equiv.) derived from 2-methyl-1-tetralone (Scheme 1).<sup>[12]</sup> However, the selectivity was disappointing. According to some of the experimental procedures of Trost and Schroeder,<sup>[13]</sup> we used LDA as a base either in THF or DME. Both experiments quantitatively afforded the alkylation product, in 5 min and 1 h, respectively, but with a low enantioselectivity (12%). Replacement of LDA with the BSA/KOAc system only led to a 2% conversion in 24 h.



Scheme 1. Palladium-catalysed asymmetric allylic alkylation of allyl acetate with 2-methyl-1-tetralone

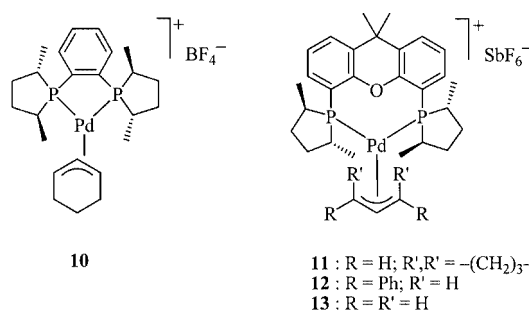
Finally, we tested the diphospholane ligands in another Pd-catalysed process, the benchmark asymmetric Heck reaction between phenyl triflate and 2,3-dihydrofuran (Scheme 2).<sup>[14]</sup> Ligand (*R,R*)-**2** associated with Pd(OAc)<sub>2</sub> as a palladium source led to very low yields and *ee* values [**8**: 5% yield, 12% *ee* (*S*); **9**: 5% yield, 2% *ee* (*R*)], whereas no reaction was observed under the same conditions with ligand (*R,R*)-**1**. With **2**, the Heck reaction with Pd(DBA)<sub>2</sub> instead of Pd(OAc)<sub>2</sub> gave racemic products in low yields (**8**: 3%; **9**: 8%).



Scheme 2. Palladium-catalysed asymmetric Heck reaction

## Allylpalladium Complexes

In order to clarify how each of the chiral diphospholane ligands affects the stereochemical outcome of the catalytic reactions, we attempted to elucidate the three-dimensional structures of some cationic allyl palladium catalytic intermediates through solid-state (crystallography) and/or solution (NMR) studies. For this purpose, a series of cationic ( $\eta^3$ -allyl)palladium complexes (**10–13**) was synthesised in acceptable to very good yields (55–93%) according to a classical procedure. Abstraction of  $\text{Cl}^-$  from the chloride-bridged dimer  $[\text{Pd}(\eta^3\text{-C}_6\text{H}_9)\text{Cl}]_2$  with  $\text{AgBF}_4$  or  $\text{AgSbF}_6$ , followed by addition of (*S,S*)-**1** or (*R,R*)-**2** afforded the cyclohexenyl complexes **10** and **11**. Complexes **12** and **13** were obtained in a similar way from (*R,R*)-**2**, starting from  $[\text{Pd}(\eta^3\text{-Ph}_2\text{C}_3\text{H}_3)\text{Cl}]_2$  or  $[\text{Pd}(\eta^3\text{-C}_3\text{H}_5)\text{Cl}]_2$ . The synthesis, NMR analysis, and X-ray structure of the related compound  $[\text{Pd}\{(R,R)\text{-Duphos}\}(\eta^3\text{-1,3-diphenylallyl})](\text{CF}_3\text{SO}_3)$  have been reported by Drago and Pregosin.<sup>[7]</sup>



## Crystallographic Studies

Single-crystals of **10** and **11** suitable for X-ray diffraction analyses were obtained from slow liquid-phase diffusion of *n*-heptane and vapour-phase diffusion of pentane, respectively, into a dichloromethane solution of the complex. The X-ray crystallographic structures are depicted in Figures 1

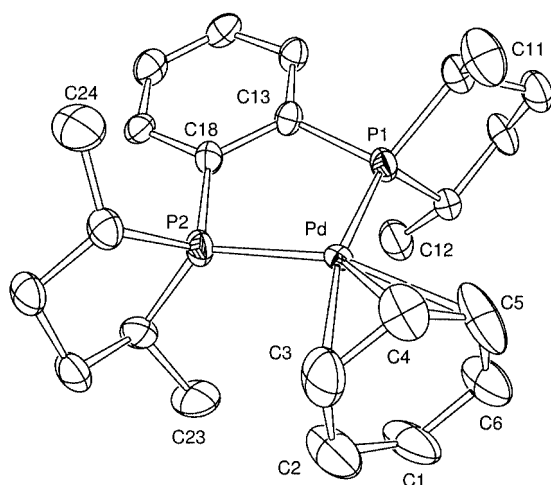


Figure 1. ORTEP drawing of  $[\text{Pd}\{(S,S)\text{-Duphos}\}(\text{C}_6\text{H}_9)](\text{BF}_4)$  (**10**) showing 30% probability thermal ellipsoids and the atom-numbering scheme; hydrogen atoms and the  $\text{BF}_4^-$  anion have been omitted for clarity

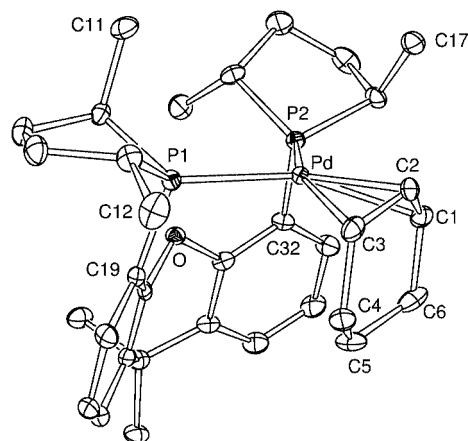


Figure 2. ORTEP drawing of  $[\text{Pd}\{(R,R)\text{-Duxantphos}\}(\text{C}_6\text{H}_9)](\text{SbF}_6)$  (**11**) showing 30% probability thermal ellipsoids and the atom-numbering scheme; hydrogen atoms and the  $\text{SbF}_6^-$  anion have been omitted for clarity

and **2** and selected bond lengths and angles are given in Tables 3 and 4. Complexes **10** and **11** crystallise as monocationic, pseudo-square-planar complexes with noncoordinating anions. Each metallic centre is coordinated by the three allylic carbon atoms and the two phosphorus atoms of the bidentate diphospholane **1** or **2**. Crystallographic disorder is present in the structure of **10**: the palladium atom occupies two positions (Pd and Pd', 50% occupancy ratio each). Pd is bound to C3, C4, and C5, whereas Pd', which is located slightly below, is bound to C6, C1, and C2. This

Table 3. Selected bond lengths [ $\text{\AA}$ ] and angles [ $^\circ$ ] in  $[\text{Pd}\{(S,S)\text{-Duphos}\}(\text{C}_6\text{H}_9)](\text{BF}_4)$  (**10**)

Pd–P1	2.278(3)	Pd–C3	2.39(2)
Pd–P2	2.323(3)	Pd–C4	2.23(1)
C3–C4	1.43(2)	Pd–C5	2.41(3)
C4–C5	1.44(3)		
P1–Pd–P2	86.40(9)	C3–Pd–C5	61.8(6)
P1–Pd–C3	167.0(4)	P2–Pd–C5	162.8(5)
P1–Pd–C5	105.5(5)	P2–Pd–C3	105.5(5)
Pd–P1–C7	117.5(3)	Pd–P2–C18	106.4(3)
Pd–P1–C10	121.6(3)	Pd–P2–C19	129.6(3)
Pd–P1–C13	107.5(3)	Pd–P2–C22	109.4(3)
C3–C4–C5	118(1)		

Table 4. Selected bond lengths [ $\text{\AA}$ ] and angles [ $^\circ$ ] for  $[\text{Pd}\{(R,R)\text{-Duxantphos}\}(\text{C}_6\text{H}_9)](\text{SbF}_6)$  (**11**)

Pd–P1	2.321(1)	Pd–C1	2.247(5)
Pd–P2	2.335(1)	Pd–C2	2.136(4)
C1–C2	1.377(8)	Pd–C3	2.206(5)
C2–C3	1.403(8)		
P1–Pd–P2	105.02(4)	C1–Pd–C3	64.9(2)
P1–Pd–C1	156.4(1)	P2–Pd–C3	156.9(1)
P1–Pd–C3	96.7(1)	P2–Pd–C1	92.0(1)
Pd–P1–C7	122.0(2)	Pd–P2–C13	116.3(2)
Pd–P1–C10	124.2(2)	Pd–P2–C16	125.7(2)
Pd–P1–C19	106.7(2)	Pd–P2–C32	107.7(2)
C1–C2–C3	118.6(5)		

disorder results in large thermal ellipsoids for the 6 cyclohexenyl carbon atoms. For the sake of clarity, only Pd is shown in Figure 1.

The overall structure of **11** is very close to the reported structure of  $[\text{Pd}\{(R,R)\text{-Duthixantphospholane}\}(\text{cyclohexenyl})]^+$ .<sup>[4a]</sup> The conformational characteristics of the Duxantphos ligand in complex **11** are similar to those of achiral xanthene-based ligands coordinated to palladium.<sup>[15,16]</sup> The main difference between **10** and **11** lies in the fact that in **10** the aromatic backbone of the ligand is approximately in the coordination plane and keeps a pseudo- $C_2$  symmetry axis, whereas in **11** the xanthene scaffold is almost perpendicular to the coordination plane. Indeed, the P1–Pd–P2 plane subtends an angle of only  $14.8(1)^\circ$  with the best-fit plane defined by the six aromatic Duphos carbons in **10**, while in **11** both xanthene aromatic rings (also defined by best-fit six-carbons planes) are bent by  $77.08(4)$  and  $75.67(4)^\circ$  with regard to the P1–Pd–P2 plane. In **11**, the tricycle is folded along an  $\text{O}\cdots\text{CMe}_2$  axis, the oxygenated six-membered ring being in a boat conformation, and the angle between the mean aromatic planes reaches  $45.32(4)^\circ$ . Another marked difference is the angle between the mean phospholane planes (defined by their five atoms) and the P1–Pd–P2 plane:  $70.6(1)$  and  $78.3(1)^\circ$  in **10** compared with only  $13.41(4)$  and  $34.52(4)^\circ$  in **11**.

The loss of symmetry of the Duxantphos ligand upon coordination to the palladium centre induces *exo/endo* isomerism in the complex. The *exo* species can be defined as the conformer where the xanthene backbone is located on the same side of the coordination plane as the cyclohexenyl or, in a more general way, where the central allylic proton is on the opposite side with regard to the backbone.<sup>[4a]</sup> It is indeed the observed conformer for **11** as well as for  $[\text{Pd}\{(R,R)\text{-duthixantphospholane}\}(\text{cyclohexenyl})]^+$ .

In both structures, the Pd–P bond lengths ( $2.278\text{--}2.335$  Å) are within the expected range for complexes with phospholanes coordinated to palladium.<sup>[4a,7,17]</sup> As expected, the bite angle P1–Pd–P2 is much larger in **11** [ $105.02(4)^\circ$ ] than in **10** [ $86.40(9)^\circ$ ]. Because of the strong *trans* influence of the phospholanes, the palladium–terminal allylic carbon bonds (**10**:  $2.39\text{--}2.41$  Å; **11**:  $2.206\text{--}2.247$  Å) are longer than in other reported Pd– $\eta^3$ -cyclohexenyl complexes.<sup>[17]</sup> In addition, they appear much longer in **10** than in **11** which is probably linked to the crystallographic disorder observed in **10** (vide supra). For the same reason, the cyclohexenyl carbons look, artificially, nearly coplanar in **10**, whereas in **11** the cyclohexenyl is in a chair conformation.

The "twist angle"  $\tau$  defined by Helmchen et al.<sup>[18]</sup> is useful here for describing the inclination of the allyl in a front view. It corresponds to the dihedral angles P1–P2–C3–C5 in **10** and P1–P2–C1–C3 in **11** and reaches the values of  $-7.0(6)^\circ$  and  $-8.7(2)^\circ$ , respectively, which are very close. In other words, in a front view of the molecule where the allyl is positioned in the foreground, the allyl appears rotated slightly clockwise so that steric interactions between it and the proximal phospholane methyls (**10**: C11 and C23; **11**: C12 and C17) are minimised. It is worth noting that within the five-membered phospholane cycles, the proximal meth-

yls of **10** are both *syn* with regard to the coordinating electron pair of the phosphorus atom, whereas in **11** C17 is *syn* but C12 is *anti*.

In **10** the mean phospholane planes are nearly parallel to the mean cyclohexenyl plane [ $5.7(2)$  and  $9.0(1)^\circ$ ] and therefore the shortest spatial distance between a terminal allylic carbon and a chiral carbon of a phospholane is  $4.015(20)$  Å (C3 $\cdots$ C22). In contrast, the phospholanes of **11** make an angle of  $72.94(5)$  and  $89.57(6)^\circ$  with the cyclohexenyl and the C3 $\cdots$ C10 and C1 $\cdots$ C13 distances are shorter at  $3.878(7)$  and  $3.548(7)$  Å, respectively. This observation mirrors exactly what Kamer et al. noted about palladium allyl complexes coordinated either by 1,2-bis(diphenylphosphanyl)ethane or xantphos.<sup>[15]</sup> The consequence is a stronger protrusion of the proximal methyls into the cyclohexenyl ligand. Their distances from the cyclohexenyl mean plane are  $2.031(2)$  Å (C12) and  $1.962(2)$  Å (C17) in **11**, compared with  $2.657(6)$  Å (C11) and  $3.428(6)$  Å (C23) in **10**. In connection with the steric repulsion between C12 and the allyl of **11**, the P1–Pd–C3 angle is slightly but significantly larger than P2–Pd–C1 [ $96.7(1)^\circ$  vs.  $92.0(1)^\circ$ ] and Pd–P1–C10 is also larger than Pd–P2–C13 [ $124.2(2)^\circ$  vs.  $116.3(2)^\circ$ ].

## NMR Investigations

We have also compared the NMR spectroscopic data of complexes **10** and **11** in solution. Like its crystallographic features, the NMR characteristics of **11** are closely akin to those of *exo*- $[\text{Pd}\{(R,R)\text{-Duthixantphospholane}\}(\text{cyclohexenyl})]^+$ . Upon coordination of the  $C_2$ -symmetric ligands **1** and **2** to the Pd centre, the loss of the symmetry axis is revealed by the  $^{31}\text{P}\{^1\text{H}\}$ ,  $^1\text{H}$ , and  $^{13}\text{C}\{^1\text{H}\}$  NMR spectra. Many signals are duplicated, e.g. the phosphorus resonances which appear as an AB system, or the four  $^1\text{H}$  NMR signals of the methyl groups borne by the phospholanes which are doublets of doublets. The  $J_{\text{P,P}}$  values measured from the  $^{31}\text{P}\{^1\text{H}\}$  spectra are slightly larger in **11** than in **10** (41 Hz vs. 36 Hz) which may be the consequence of an increased P–Pd–P angle.

The chemical shifts of the phosphorus nuclei are higher in the Duphos complex **10** ( $\delta = 68.2$  and  $71.9$  ppm) than in the Duxantphos complex **11** ( $\delta = 33.7$  and  $35.5$  ppm). This deshielding could be expected in view of the ring contribution ( $\Delta_{\text{R}}$ ) parameter<sup>[19]</sup> which reaches a high value for a five-membered metallacycle. The chemical shift difference between the terminal allylic  $^{13}\text{C}$  signals is a useful tool to account for asymmetry in the allyl bonding.<sup>[7]</sup> Here, we observed that this difference is only  $\Delta\delta = 5.2$  ppm in **10**, but reaches  $\Delta\delta = 12.0$  ppm in **11**.

The case of complex  $[\text{Pd}\{(R,R)\text{-2}\}(\eta^3\text{-1,3-diphenylallyl})](\text{SbF}_6)$  (**12**) appears to be more complicated. In spite of numerous efforts, we did not manage to grow single crystals for X-ray analysis. Its room-temperature  $^{31}\text{P}\{^1\text{H}\}$  and  $^1\text{H}$  NMR spectra exhibit broad signals which sharpen when the

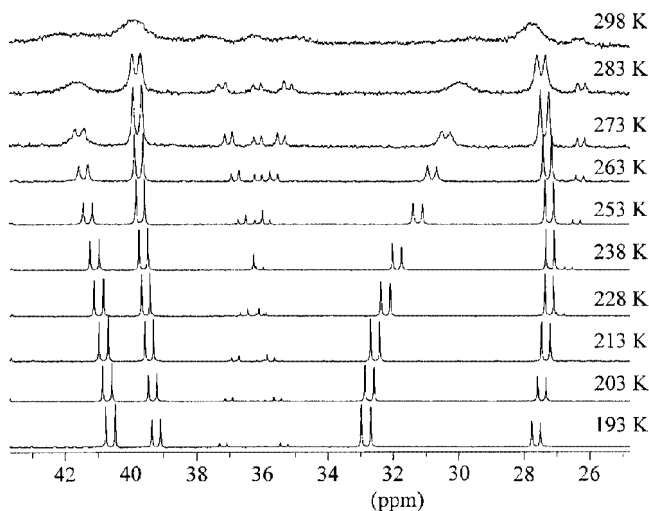
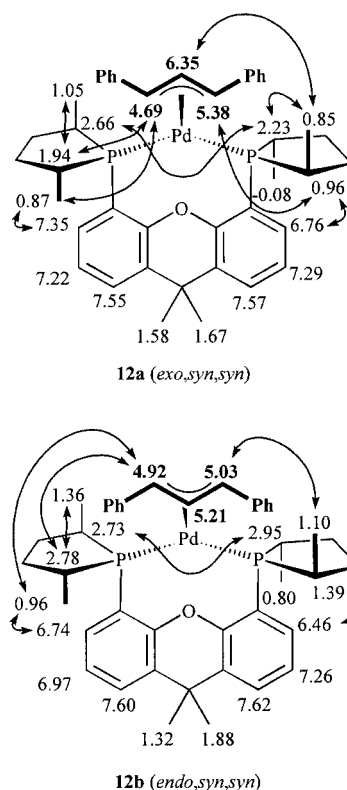


Figure 3. 202.5 MHz  $^{31}\text{P}\{^1\text{H}\}$  NMR spectra of  $[\text{Pd}\{(\text{R,R})\text{-Duxantphos}\}(\text{Ph}_2\text{C}_3\text{H}_3)](\text{SbF}_6)$  (**12**) in  $\text{CD}_2\text{Cl}_2$  in the range 193–298 K

temperature is decreased (Figure 3). Below 273 K, the  $^{31}\text{P}$  NMR spectra exhibit eight narrow doublets between  $\delta = 26$  and 42 ppm with  $45 \text{ Hz} < J_{\text{P,P}} < 57 \text{ Hz}$ , values which are all close to those found for complex **11**. Measurement of the P–P coupling constants associated with a  $^{31}\text{P}\{^1\text{H}\}$  COSY spectrum recorded at 193 K allowed us to identify them as four AB systems, corresponding to two major (**12a,b**) and two minor (**12c,d**) isomeric species where a Pd atom is chelated by the diphospholane. If we assume that we can rely on the integration of the  $^{31}\text{P}\{^1\text{H}\}$  NMR signals, their relative ratios are 35:25:4:1 at 193 K. **12a** and **12b** are predominant whatever the temperature. Coalescence of the  $^{31}\text{P}$  and  $^1\text{H}$  signals of the four isomers upon warming to room temperature indicates that they undergo fast exchange processes.

2D- $^1\text{H}$  NMR spectroscopy has proved to be a very useful tool for the investigation of the 3D structures of allyl Pd complexes.<sup>[3]</sup> Indeed, although many signals of the 1D- $^1\text{H}$  NMR spectrum of **12** recorded at 193 K overlap, 2D-NMR analysis combined with phosphorus-decoupled proton NMR spectroscopy allowed us to assign most of the signals of both major isomers and identify them as *exo,syn,syn* (**12a**) and *endo,syn,syn* (**12b**) (Scheme 3). In each isomer, all the  $^1\text{H}$  signals of the diphospholane ligand (except the methylene signals) could be assigned with the help of 2D- $^1\text{H}$  COSY and ROESY spectra, each proton being connected to another by scalar coupling and/or by spatial proximity (NOE effect). The aromatic protons located in the *ortho* position with regard to the phospholane substituents are characterised by a  $^3J_{\text{H,P}}$  value of ca. 7 Hz. We can unambiguously identify the signals of the key proximal phospholane methyl groups that point in the foreground towards the allyl moiety. In the 2D- $^1\text{H}$  ROESY spectrum, the left-side proximal methyl group displays a strong NOE with the adjacent *ortho*-xanthene proton (e.g. at  $\delta = 7.35$  ppm in the *exo* isomer), whereas the other *ortho* proton (e.g. *exo*:  $\delta = 6.76$  ppm) shows an NOE with the methylidyne group that

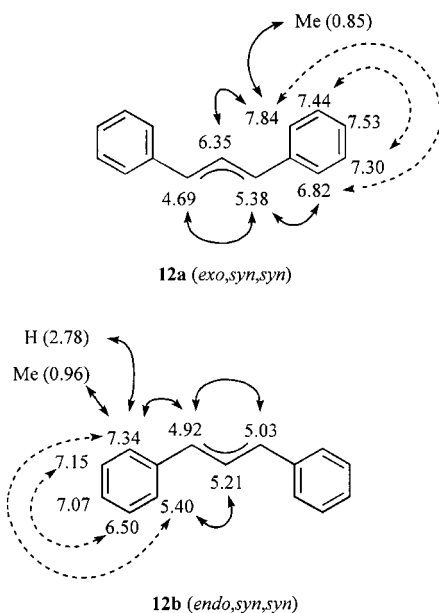


Scheme 3. Representation of relevant NOE contacts in **12a** and **12b** from  $^1\text{H}$  ROESY; for the sake of clarity, NOEs associated with scalar couplings are not shown

is geminal with the right-side proximal methyl group. In the background, NOEs are observed between both phospholane distal methylidyne groups (e.g. *exo*:  $\delta = 2.23$  and 2.66 ppm) which is an indication that the xanthene backbone is folded as in the X-ray structure of **11**.

Six allyl signals are spread over a rather large range, i.e.  $\delta = 4.69\text{--}6.35$  ppm. The *syn,syn* geometry of the allyl ligand was established in both isomers from NOE cross-peaks between the lateral allyl signals ( $\delta = 4.69\text{--}5.38$  and  $4.92\text{--}5.03$  ppm; see Scheme 4). This is also suggested by the large values of the coupling constants between the central and lateral allylic protons (10–14 Hz), although this fact alone would not be definite proof.<sup>[3a]</sup> We note, however, that within each allyl ligand, both values of  $^3J_{\text{H,H}}$  are not equal which suggests that the allyl group undergoes deformations.

The assignment of the allyl configuration (*exo* or *endo*) is essentially based on the interligand NOEs that the lateral-right and central allylic protons cause or do not cause with the right-side proximal phospholane methyl group and its *gem*-methylidyne group (Scheme 3). The *endo* structure of isomer **12b** is supported by the very intense NOE cross-peak of the allyl proton signal at  $\delta = 5.03$  ppm with the methyl signal at  $\delta = 1.10$  ppm (Figure 4). In the *exo* isomer **12a**, the lateral allyl proton ( $\delta = 5.38$  ppm) shows a close NOE contact with the proximal methylidyne group ( $\delta = 0.96$  ppm) but not with the methyl group ( $\delta = 0.85$  ppm). In addition, an NOE signal between the *exo* central allyl signal at  $\delta = 6.35$  ppm and the proximal methyl signal at



Scheme 4. Representation of relevant NOE contacts (plain arrows) and chemical exchanges (broken arrows) within the allyl ligand in **12a** and **12b** from ROESY experiments; for the sake of clarity, NOEs associated with scalar couplings are not shown

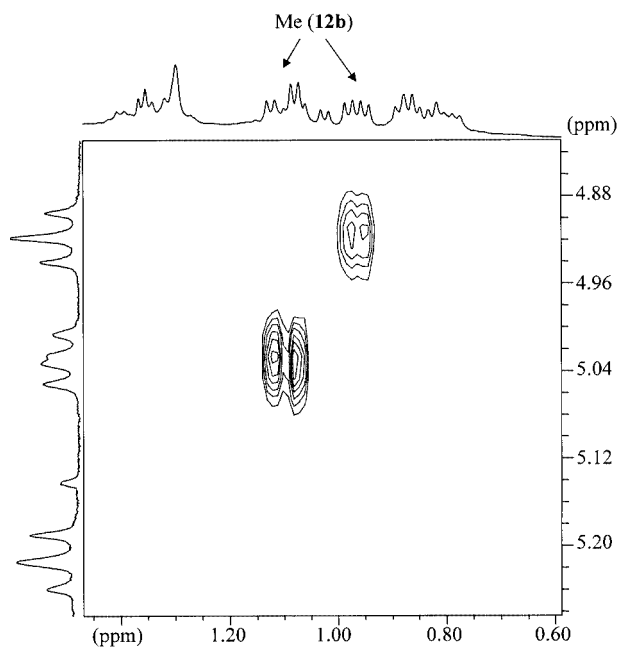


Figure 4. Section of the  $^1\text{H}$  ROESY spectrum of **12** recorded in  $\text{CD}_2\text{Cl}_2$  at 193 K; a section of the aliphatic region is represented horizontally and the three allylic proton signals of **12b** vertically

$\delta = 0.85$  ppm can be observed. However, **12a** and **12b** cannot be differentiated by the left-side lateral allylic proton (**12a**:  $\delta = 4.69$  ppm; **12b**:  $\delta = 4.92$  ppm) because they both display NOEs with the proximal, left-side methyl group and methyldyne group.

The low frequency shift of some of the protons is consistent with their positioning in the anisotropy cone of the aromatic rings. The *exo* central allylic proton resonates in the

normal range ( $\delta = 6.35$  ppm). In comparison, the chemical shift of the central proton of  $[\text{Pd}(\text{Duphos})(1,3\text{-diphenylallyl})]^+$  is  $\delta = 6.84$  ppm, although the signal of the homologous proton of the *endo* isomer that lies in the anisotropy cone of both xanthene aromatic cycles is shifted upfield by more than 1 ppm ( $\delta = 5.21$  ppm). Conversely, the signals of several protons belonging to the diphospholane ligand are shifted upfield, such as (1) on the right side of the *exo* isomer, the *ortho*-xanthene proton ( $\delta = 6.76$  ppm), the proximal methyldyne group ( $\delta = 0.96$  ppm) and even the distal methyl group ( $\delta = -0.08$  ppm) as well as (2) on the *endo* isomer, both *ortho*-xanthene protons ( $\delta = 6.46$  and  $6.74$  ppm) and the proximal methyldyne group on the right ( $\delta = 1.39$  ppm). These shifts are probably related to the anisotropy cone of the phenyl substituents of the allyl moiety.

In each isomer, only the  $^1\text{H}$  signals of one phenyl substituent can be identified, i.e. the right-side phenyl group in the *exo* form and the left-side one in the *endo* form (Scheme 4). For each of them, five distinct resonances can be observed. This means that their rotation is frozen at 193 K because of the steric effect of the proximal methyl groups. However, positive exchange (EXSY) cross-peaks related to this rotation, between the *ortho* and *meta* protons of each phenyl group, can be found in the  $^1\text{H}$  ROESY spectrum. The protons oriented downwards resonate at low frequencies (e.g. the *endo,ortho* proton signal at  $\delta = 5.40$  ppm) because of their location in the anisotropy cone of the xanthene backbone (vide supra).

The  $^1\text{H}$  NMR signals of both minor isomers **12c** and **12d** could hardly be detected in the spectra because of overlapping of the signals of the major isomers **12a** and **12b**. However, in view of related (1,3-diphenylallyl)palladium complexes,<sup>[3]</sup> it seems highly probable that they are *syn,anti* isomers (vide infra). Such *syn,anti* (1,3-diphenylallyl)palladium complexes are generally less stable than *syn,syn* isomers because of unfavorable  $\text{Ph}_{\text{anti}}-\text{H}_{\text{anti}}$  steric interactions.

From the integration of the respective  $^1\text{H}$  NMR signals of **12a** and **12b** in  $\text{CD}_2\text{Cl}_2$ , we observed that the  $[\mathbf{12a}]/[\mathbf{12b}]$  ratio in solution increased with the temperature and that a plot of  $\ln K$  ( $K = [\mathbf{12a}]/[\mathbf{12b}]$ ) vs.  $1/T$  is a straight line (Figure 5). This allowed us to estimate the thermodynamic data of the equilibrium, viz.  $\Delta H^\circ \approx 4 \text{ kJ}\cdot\text{mol}^{-1}$  and  $\Delta S^\circ \approx 18 \text{ J}\cdot\text{mol}^{-1}\cdot\text{K}^{-1}$ . Upon warming from 193 to 298 K, the intensity of the AB system at  $\delta \approx 28$  and 39 ppm in the  $^{31}\text{P}$  NMR spectrum increased, whereas that of the AB pattern at  $\delta \approx 31\text{--}33$  and 40–42 ppm decreased (Figure 3). We can, therefore, assign the first couple of signals to **12a** and the second to **12b**, by comparison with the variable-temperature  $^1\text{H}$  NMR spectroscopic data.

The broadening of the  $^1\text{H}$  and  $^{31}\text{P}\{^1\text{H}\}$  NMR signals of **12** upon increasing the temperature from 193 K to room temperature is characteristic of fluxional processes. We tried to record a high-temperature (323 K)  $^{31}\text{P}\{^1\text{H}\}$  NMR spectrum of **12** in  $\text{CD}_3\text{NO}_2$  but unfortunately it decomposed upon heating before any narrowing of the signals could be observed. We envisioned that the equilibria between the isomers of **12** could be visualised by low-temperature 2D

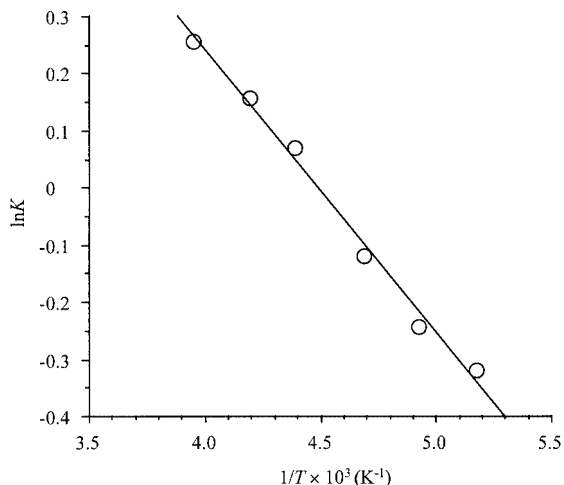


Figure 5.  $\ln K$  vs.  $1/T$  curve ( $K = [12a]/[12b]$  in  $CD_2Cl_2$ )

exchange NMR spectroscopy. No exchange cross-peaks involving allylic protons were found in the  $^1H$  ROESY spectrum, probably because the exchange rates are too low at 193 K. However, we could observe two cross-peaks which reveal very selective chemical exchanges of phosphorus nuclei in a  $^{31}P\{^1H\}$  ROESY spectrum recorded at 263 K (Figure 6). This can be interpreted as the consequence of a conformational equilibrium between the major isomers **12a**

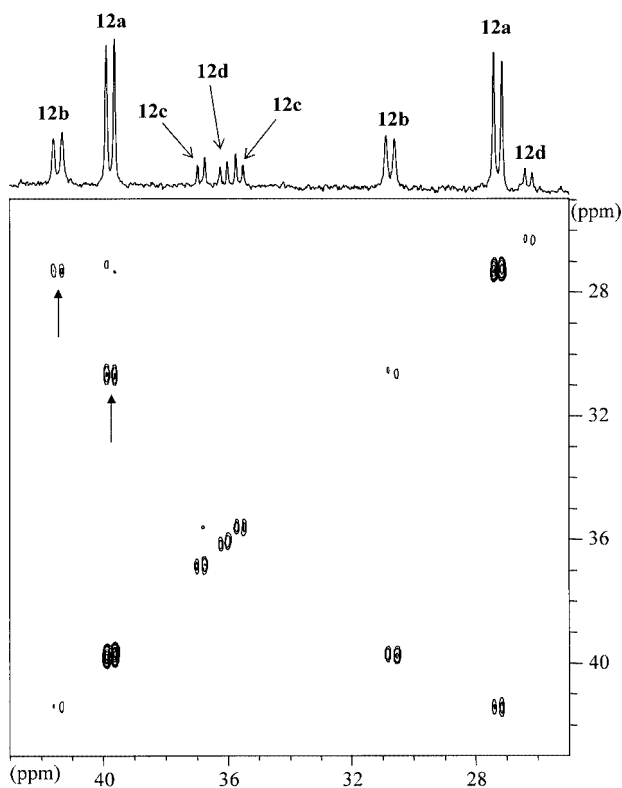
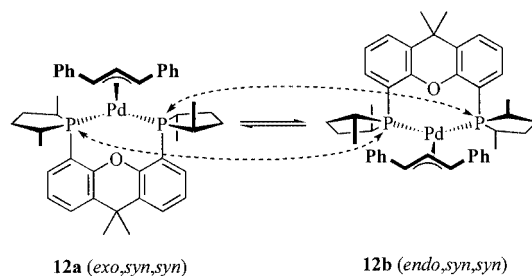


Figure 6.  $^{31}P$  ROESY spectrum of **12** recorded in  $CD_2Cl_2$  at 263 K; exchange cross-peaks between **12a** and **12b** are designated by arrows



Scheme 5. Hypothetical conformational equilibrium between **12a** and **12b** accounting for the phosphorus nuclei exchanges (broken arrows) observed by  $^{31}P$  ROESY

and **12b** (Scheme 5), where the xanthene backbone moves upwards rotating around the  $P\cdots P$  axis (flip-flop). Very similar NMR observations of a  $Pd(\text{diphosphane})(\eta^3\text{-allyl})$  complex have been reported.<sup>[20]</sup> No exchange cross-peaks were found in the  $^{31}P$  ROESY spectrum between the signals of the major *syn,syn* and the minor hypothetically *syn,anti* isomers, which means that  $\eta^3-\eta^1-\eta^3$  isomerization is too slow to be observed at 263 K. It is plausible that this process, which involves  $Pd-C$  bond breaking, is slower than a conformational equilibrium.

A  $^{13}C\{^1H\}$  NMR spectrum of **12** was recorded at 263 K in  $CD_3NO_2$ , a solvent in which the complex is reasonably soluble (a spectrum recorded in  $CD_2Cl_2$  resulted in a poor signal-to-noise ratio). Although the spectrum is complicated because many species are present in solution, we assigned the most intense signals to **12a** which is by far the predominant species at this temperature. One of the terminal allylic carbon atoms has olefin-like character<sup>[3b]</sup> with a high-frequency chemical shift of  $\delta = 100.2$  ppm. As in the cyclohexenyl series, the  $\Delta\delta_C$  terminal allyl value is much larger with Duxantphos ( $\delta = 22.4$  ppm) than with Duphos ( $\delta = 10.3$  ppm<sup>[7]</sup>). Indeed,  $\delta = 22.4$  ppm is particularly high for a (1,3-diphenylallyl) $Pd$  complex chelated by two donor atoms of the same type.<sup>[3b]</sup> The terminal allyl carbon signals of **12a** are doublets (as in the cyclohexenyl analogue **11**) and the coupling constants with their respectively *trans*-positioned phosphorus atom are quite different ( $\delta = 77.8$  ppm, 30 Hz vs.  $\delta = 100.2$  ppm, 20 Hz). All these observations are consistent with an allyl deformation or tilt which was suggested by the values of the H-H coupling constants within the allyl (vide supra).

Like **12**, complex  $[Pd(R,R)\text{-}2](\eta^3\text{-allyl})(SbF_6)$  (**13**) could not be analysed by X-ray crystallography. Instead, a detailed NMR spectroscopic analysis was carried out. Its low-temperature  $^{31}P\{^1H\}$  NMR spectrum revealed the presence of *exo* and *endo* isomers in very different proportions, i.e. with a ratio  $> 10$  (Figure 7). At 183 K, the major compound was characterised by an AB system at  $\delta = 33.2$  and 34.3 ppm ( $J_{P,P} = 40$  Hz), whereas only one doublet of the minor species was visible at  $\delta = 31.3$  ppm ( $J_{P,P} = 40$  Hz). Upon heating, we observed a coalescence of the signals which led to a single averaged AB system at room temperature. The coalescence temperature can be roughly estimated as 223 K. This suggests that the energy barrier of the fluxional process is lower for **13** than for **12**. A straightfor-

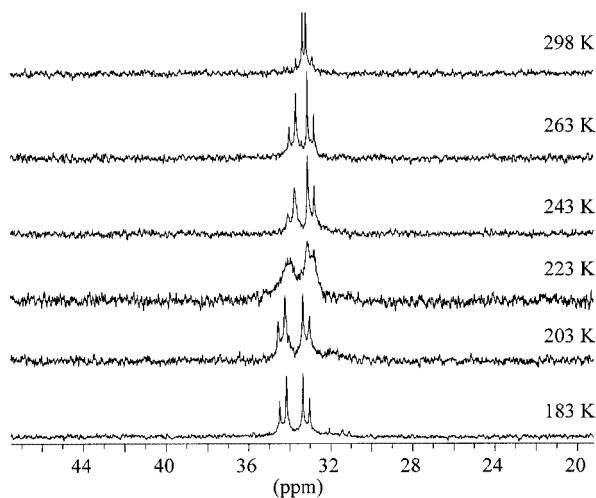
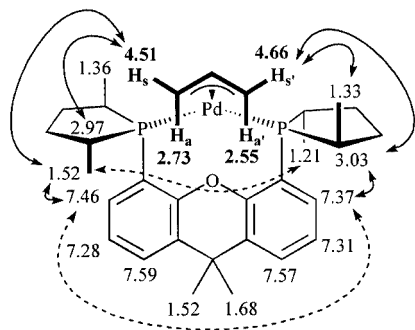


Figure 7. 121.5 MHz  $^{31}\text{P}\{^1\text{H}\}$  NMR spectra of  $[\text{Pd}\{(R,R)\text{-Duxantphos}\}(\text{C}_3\text{H}_5)](\text{SbF}_6)$  (**13**) in  $\text{CD}_2\text{Cl}_2$  in the range 183–298 K

ward explanation based on the steric effect of the bulky 1,3-diphenylallyl moiety can be proposed.

It is highly probable that the major species at low temperature is also largely predominant at room temperature, i.e. above the coalescence temperature. Therefore, the diagnostic cross-peaks observed in the  $^1\text{H}$  ROESY NMR spectrum recorded at room temperature must be characteristic of that major isomer. Most of the protons of Duxantphos in **13** could be identified with the help of that spectrum, in connection with key  $\text{Me}\cdots\text{H}_{\text{ar}}$  and  $\text{CH}\cdots\text{H}_{\text{ar}}$  NOE cross-peaks. Several indications tend to show that it corresponds to the *exo* isomer shown in Scheme 6. In an *endo* isomer, a strong NOE interaction between  $\text{H}_{\text{anti}}$  ( $\delta = 2.55$  ppm) and the phospholane methyl group ( $\delta = 1.33$  ppm) on the right side would be expected, which is not the case. Furthermore, by comparison with reported  $[\text{Pd}(\text{trialkylphosphane})_2(\text{allyl})]^+$  complexes,<sup>[21]</sup> the chemical shifts of the *anti* protons are rather low, possibly because they are located in the anisotropy cone of the backbone aromatic rings in the *exo* conformation. Unfortunately, this assignment is not unambiguous, since each allylic *syn* proton displays NOEs with



Scheme 6. Representation of relevant NOE contacts (plain arrows) and chemical exchanges (broken arrows) in **13** from  $^1\text{H}$  ROESY; for the sake of clarity, NOEs associated with scalar couplings are not shown

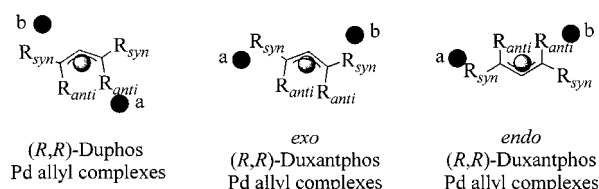
a methyl group and a methylidyne group, whereas the allylic *anti* or central protons show no significant NOE with any of the Duxantphos protons.

We found two distinct chemical exchange (positive) cross-peaks in the ROESY spectrum between both *ortho*-xanthene protons and also between two methyl groups (Scheme 6). Other exchange cross-peaks involving Duxantphos protons could not be distinguished because the chemical shifts of the exchanging nuclei were too close. Besides, the four terminal allyl protons all exchange with each other. All these exchange cross-peaks can be interpreted as the result of a flip–flop of the diphospholane ligand similar to that shown in Scheme 5 (leading to the minor isomer), followed by an isomerization back to the major species through a classical  $\eta^3-\eta^1-\eta^3$  allyl rearrangement mechanism.<sup>[1b]</sup>

## Discussion

The purpose of this discussion is to try to establish a link between the structural information provided by the analysis of allyl palladium complexes and some of our most valuable results of palladium-catalysed allylic alkylations with diphospholane ligands, i.e. with substrates **3a** and **3c**.

As a result of the bite angle of the diphospholane, the conformation of the scaffold generates *exo/endo* isomerism in the Duxantphos complexes **11–13** and both forms are in equilibrium. In contrast, Duphos maintains a pseudo- $C_2$  symmetry when it is coordinated to the metal atom and there is no such isomerism. We have represented, in Scheme 7, some simplified front views of the allyl palladium complexes, in analogy with previously reported representations.<sup>[4]</sup> This allows us to visualise the interactions of the proximal methyl groups of the (*R,R*)-diphospholane ligands with the allyl moiety. The proximal methyl groups [(a) = down; (b) = up] have dramatically different positions depending on the ligand: with (*R,R*)-Duphos, (a) is on the right and (b) on the left, whereas the reverse is true with (*R,R*)-Duxantphos. However, this picture does not account for the distances between the methyl groups and the allyl plane which are shorter with Duxantphos than with Duphos (vide supra).



Scheme 7. Front-view representation of  $[\text{Pd}(\text{diphospholane})(\text{allyl})]^+$  complexes; black circles = proximal methyl groups; gray circle = palladium centre

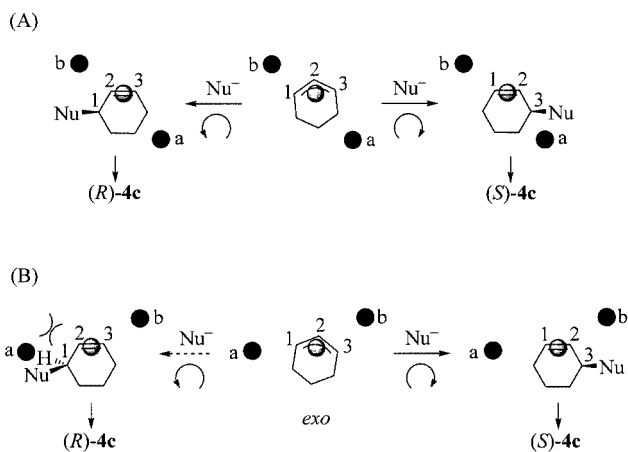
The example of the cyclohexenyl complex **11** {or of  $[\text{Pd}\{(R,R)\text{-Duthixantphospholane}\}(\text{cyclohexenyl})]^+$  [4a]}, indicates that a methyl group (b) cannot accommodate an

*anti* substituent on the right in the *endo* isomer. Therefore, an *endo* isomer of **11** could not be detected. On the other hand, when the allyl group is *syn,syn*-substituted with large phenyl groups (complex **12**), the *exo* and *endo* forms coexist in comparable proportions. Both undergo some internal steric congestion, as illustrated by the restricted rotation of some phenyl groups because of the proximity of phospholane methyl groups (Scheme 4, *vide supra*). *syn,anti* 1,3-Diphenylallyl complexes are normally destabilised by  $H_{anti}-Ph_{anti}$  steric repulsion but can be present in significant quantity with a large, intrusive ancillary ligand.<sup>[22]</sup> Indeed, minor isomers of **12**, which are very probably *syn,anti*, coexist with the major *syn,syn* isomers, whereas  $[Pd(Duphos)(\eta^3-1,3\text{-diphenylallyl})]^+$  is exclusively *syn,syn*,<sup>[7]</sup> in connection with the fact that Duphos is less intrusive than Duxantphos. When Ph is replaced by a smaller Me on the Duxantphos complex, the *syn,anti* species become predominant.<sup>[4b]</sup> In brief, it appears that the proportion of each stereoisomer of a given allyl complex, whether it is related to *exolendo* or to *syn/anti* isomerism, is the result of a subtle balance between various steric effects.

A general trend in our catalytic results in the field of allylic alkylation is a higher reactivity of ligand **2** compared with ligand **1**. Here, the reaction rate increases with the bite angle. Such an effect has already been reported in Pd-catalysed allylic alkylations, but it is not always the rule.<sup>[15,23]</sup> It can be interpreted as the consequence of a greater stability of the  $Pd^0$ -alkene complex which results from the nucleophilic attack on a  $Pd^{II}$ -allyl species, assuming that it is the rate-limiting step of the catalytic cycle.<sup>[24a]</sup> The origin of this stabilisation can be interpreted as the result of a decrease of the HOMO energy level, as suggested by Walsh diagrams.<sup>[6a]</sup>

With substrates that generate a symmetrically substituted  $\eta^3$ -allyl ligand (*viz.* substrates **3a–d**), the enantioselectivity of the catalytic process arises from the regioselectivity of the nucleophilic attack where the  $Pd^{II}$ - $\eta^3$ -allyl complex is converted into a  $Pd^0$ - $\eta^2$ -alkene complex. An interpretation of the origin of the enantioselectivity is provided by the concept of preferential rotation of the allyl group,<sup>[4,9]</sup> also referred to as torquoselectivity.<sup>[25]</sup> This interpretation is based on the hypothesis of a medium to late transition state<sup>[24]</sup> in which unhindered, thermodynamically more stable  $Pd^0$ -olefin products would be favoured. In the present case, enantiodiscrimination is governed by steric interactions between the proximal methyl groups and the coordinated alkene product (Schemes 7 and 8).

An explanation that accounts for the catalytic superiority of **2** over **1** with **3c** as the substrate is given in Scheme 8. In Scheme 8A, the methyl group (a) of (*R,R*)-Duphos is located low and far from the allylic carbon atoms and interacts very little with the cyclohexenyl moiety. Therefore, no major steric clash is expected whether the allyl group rotates clockwise or anticlockwise. This correlates well with the poor enantioselectivity of the reaction (5% *ee*). On the contrary, the situation with (*R,R*)-Duxantphos is the same as with (*R,R*)-Duthixantphos.<sup>[4]</sup> That is, an anticlockwise rotation is unfavourable because of the steric strain between



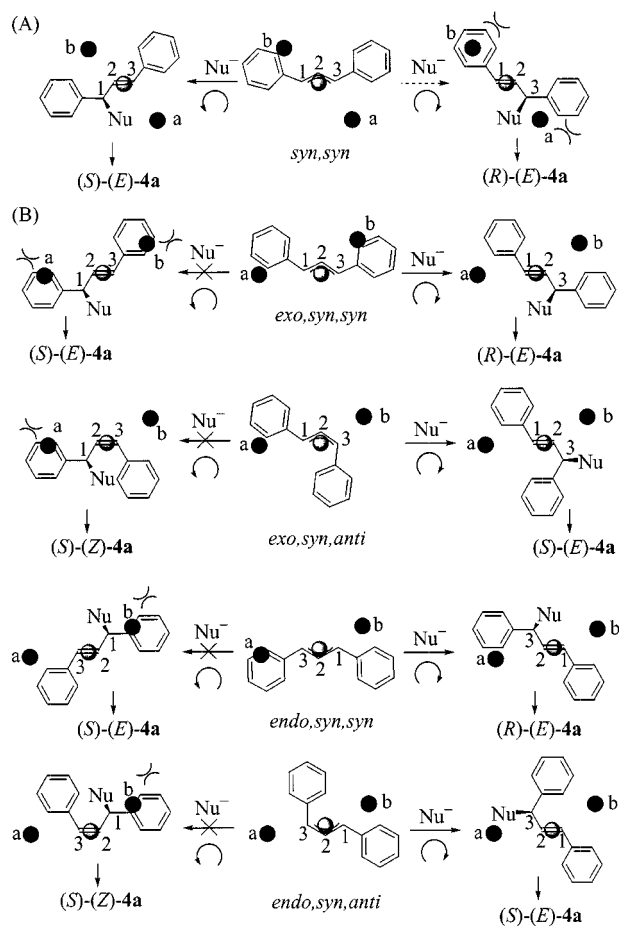
Scheme 8. Interpretation of the selectivity of the nucleophilic attack of the  $Pd$ -cyclohexenyl intermediate with (A) (*R,R*)-**1** or (B) (*R,R*)-**2** as ligands; Nu =  $CH(COOMe)_2$

C1–H and the methyl group (a) in the  $Pd^0$ -olefin species, whereas no such strain hinders a clockwise rotation of the allyl group (Scheme 8B). Indeed, compound (*S*)-**4** is formed with a high *ee* (83%) in the catalytic process run with ligand (*R,R*)-**2**.

It has been reported that in palladium-catalysed asymmetric allylic alkylation, a twist of the allyl group (observed by X-ray crystallography) toward a product-like state might influence the regioselectivity of the nucleophilic attack.<sup>[16,24c]</sup> However, in complex  $[Pd\{(R,R)\text{-Duphos}\}(\text{cyclohexenyl})]^+$  which is the mirror image of **10**, the allyl group is twisted anticlockwise according to the crystal structure of **10**. Nevertheless, a clockwise rotation is slightly favoured. Hence, this is another argument against an early transition state with these ligands.

With the encumbered substrate **3a**, chirality transfer was very efficient in the catalytic reaction. The configurations of **4a** were found to be opposite with both diphospholane ligands, obviously because the positions of the proximal methyl groups (a) and (b), which undergo repulsive interaction with the phenyl substituents, are inverse (Scheme 9). If the nucleophile attacks the C3 atom of  $[Pd\{(R,R)\text{-Duphos}\}(\text{cyclohexenyl})]^+$ , a very severe steric clash occurs between barrier (b) and the left-side phenyl group and, to a lesser extent, between barrier (a) and the right-side phenyl group (Scheme 9A). Nucleophilic attack at C1 accompanied with anticlockwise rotation of the allyl group does not experience a high energy barrier related to steric strain. This is in agreement with the formation of (*S*)-**4a** with 97% *ee*.

Things are more complicated with Duxantphos, with 4 diastereomers of the 1,3-diphenylallyl complex **12** being detected by  $^3P\{^1H\}$  NMR spectroscopy (Scheme 9B). It is reasonable to suppose that the minor isomers **12c** and **12d** are the two *syn,anti* species shown in Scheme 9 (among four possible isomers), where no major steric clash exists between the proximal methyl groups and the phenyl substituents. *cis*-**4a** was not detected in the catalysed reaction. This implies that anticlockwise rotation upon nucleophilic attack



Scheme 9. Interpretation of the selectivity of the nucleophilic attack of the Pd-1,3-diphenylallyl intermediate with (A) (*R,R*)-**1** or (B) (*R,R*)-**2** as ligands; Nu = CH(COOMe)<sub>2</sub>

of the *syn,anti* allyl complexes is forbidden because of steric repulsion of one of the phenyl groups with the methyl group (a) (*exo*) or (b) (*endo*). This raises the question as to why a sterically hindered movement of the allyl group is forbidden and not just slowed down. We propose two arguments to explain this: (1) from the comparison with the Duxantphos cyclohexenyl complex, it appears that the *syn* substituent is a bulky phenyl group and not a proton and (2), as stated above, the proximal methyl groups of Duxantphos are much closer to the allyl plane than those of Duphos. Since the environment of C1 is the same in the *exo,syn* and the *exo,syn,anti* species represented in Scheme 9, an anticlockwise rotation of the *exo,syn,anti* allyl group must also be forbidden. The same reasoning is valid for the *endo* species.

Hence, only clockwise rotations occur in the four isomers of **12**, in analogy with the interpretation reported for the 1,3-dimethylallyl system.<sup>[4b]</sup> Both major *syn,anti* isomers lead to the (*R*) alkylated product, whereas the minor *syn,anti* species lead to the (*S*) product. Our interpretation based on the hypothesis of Curtin–Hammett conditions<sup>[24a]</sup> is in agreement with the high measured *ee* values (85–89%) of (*R*)-**4a**. In comparison with the case of Duphos, the presence of *syn,anti* catalytic intermediates is detrimental to the enantioselectivity. We are, however,

aware that the interpretation proposed here is qualitative since we know nothing of the relative nucleophilic attack rate on each diastereomer of **12**. In particular, it looks probable that this rate is superior for **12a** than for **12b**: in the latter, a clockwise rotation may be somewhat hindered by the methyl group (a).

## Conclusion

In this paper we have compared the catalytic and structural properties of the two chiral diphospholane ligands coordinated to Pd, viz. **1** and **2** which differ in their bite angle. Palladium-catalysed allylic alkylation tests have confirmed the success of xanthene-based diphospholane with the “symmetrical” allylic substrates **3a–d**<sup>[4]</sup> but this success was found to be somewhat limited. Attempts to use other kinds of substrates or nucleophiles, for example, led to modest selectivities at best. However, a strong positive bite angle effect was found in allylic alkylation with small, sterically unhindered substrates such as **3b–d**, where Duxantphos was much superior to Duphos in terms of reactivity and especially enantioselectivity.

Investigations of the 3D structures of the allyl complexes **10–13** were carried out by NMR spectroscopy and, whenever possible, by X-ray crystallography. Overall, these analyses have provided accurate indications about the structural differences between Duphos and Duxantphos. The increase in the bite angle induces a loss of C<sub>2</sub> symmetry of the ligand upon coordination and renders its proximal methyl groups more intrusive towards the allyl group. These differences have major consequences on the nature and distribution of the Pd–allyl intermediates and, furthermore, on the intimate mechanism of catalytic selectivity which is based on steric factors. We applied the preferential rotation concept which proved to be a very suitable model to account for the catalytic results. With (*R,R*)-Duxantphos, we found that a clockwise rotation in the nucleophilic attack step is the preferred, and sometimes the exclusive motion of the allyl group. (*R,R*)-Duphos, on the other hand, leads to anticlockwise rotation but only if the allyl group carries bulky phenyl substituents. In conclusion, the comparison of Duphos (**1**) with Duxantphos (**2**) emphasises the advantages of large bite angle ligands.

## Experimental Section

**General Procedures:** All experiments were carried out under nitrogen or argon using a vacuum line or Vacuum Atmospheres glovebox equipped with a Dri-Train HE-493 inert gas purifier. Pentane, benzene, diethyl ether, and THF were distilled from sodium and benzophenone whereas acetonitrile and dichloromethane were distilled over calcium hydride under nitrogen immediately before use. Column chromatography was carried out on Merck silica gel 60, 70–230 mesh ASTM and thin layer chromatography on Macherey–Nagel 0.25 mm Polygram® Sil G/UV<sub>254</sub> precoated silica gel plates. Commercial reagents were used as received: Strem: (*R,R*)- and (*S,S*)-Duphos, AgBF<sub>4</sub>; Aldrich: dimethyl malonate,

*N,O*-bis(trimethylsilyl)acetamide (BSA), potassium acetate, (*rac*)-2-methyl-1-tetralone, allyl acetate, 2,3-dihydrofuran, phenyl triflate, *N,N*-diisopropylethylamine, europium tris[3-(heptafluoropropylhydroxymethylene)-(+)-camphorate] [Eu(hfc)<sub>3</sub>], AgSbF<sub>6</sub>; Prolabo: *n*-heptane. NaH (60% in mineral oil; Fluka) was washed three times with pentane, dried in vacuo, and stored in the glovebox. (*R,R*)-Duxantphos was prepared according to ref.<sup>[4]</sup> The compounds listed hereafter were synthesised according to reported procedures: (*rac*)-(*E*)-1-acetoxy-1,3-diphenylprop-2-ene (**3a**),<sup>[26]</sup> (*rac*)-(*E*)-2-acetoxyprop-3-ene (**3b**),<sup>[27]</sup> (*rac*)-1-acetoxycyclohex-2-ene (**3c**),<sup>[28]</sup> (*rac*)-1-acetoxycyclopent-2-ene (**3d**),<sup>[29]</sup> (*rac*)-(*E*)-2-acetoxy-4-phenylbut-3-ene (**5a**),<sup>[8]</sup> (*rac*)-(*E*)-3-acetoxy-2-methylhex-4-ene (**5b**),<sup>[30]</sup> bis[(η<sup>3</sup>-allyl)chloropalladium],<sup>[31]</sup> bis[(η<sup>3</sup>-cyclohexenyl)chloropalladium],<sup>[32]</sup> bis[(η<sup>3</sup>-1,3-diphenylallyl)chloropalladium],<sup>[24]</sup> NMR spectra were recorded at room temperature (unless otherwise indicated) with Bruker spectrometers. <sup>1</sup>H NMR spectra were recorded at 300.16 MHz (AC-300 instrument) or 500.13 MHz (ARX-500) and referenced to SiMe<sub>4</sub>. The assignments and measurements of coupling constants were supported by irradiations. <sup>1</sup>H{<sup>31</sup>P}, <sup>1</sup>H COSY, and/or <sup>31</sup>P{<sup>1</sup>H} COSY spectra were recorded with the ARX-500 instrument. <sup>13</sup>C{<sup>1</sup>H} NMR spectra (broadband-decoupled) were recorded at 75.48 MHz (AC-300), 100.62 MHz (AM-400), or 125.76 MHz (ARX-500) and referenced to SiMe<sub>4</sub>. The assignments were supported by DEPT-135°. <sup>31</sup>P{<sup>1</sup>H} spectra (broadband-decoupled) were recorded at 121.51 MHz (AC-300) or 202.46 MHz (ARX-500) and referenced to 85% aqueous H<sub>3</sub>PO<sub>4</sub>. The phase-sensitive 2D ROESY spectra<sup>[33]</sup> were recorded with the ARX-500 spectrometer using mixing times of 0.25 s (<sup>1</sup>H) or 0.1 s (<sup>31</sup>P{<sup>1</sup>H}). FAB MS spectra were carried out at the corresponding facilities at the Fédération de Recherche de Chimie, Université Louis Pasteur, Strasbourg and elemental analyses by the Service Central d'Analyses, CNRS, Vernaison. Optical rotations were checked with a Perkin–Elmer Otopol III polarimeter (λ = 589 nm). GC analyses were performed with a Hewlett Packard 5890 series II apparatus equipped with a 30 m × 0.25 mm SGE 25QC2 capillary column (for conversion measurements) or with a 30 m × 0.25 mm Restek Rt-βDEXse capillary column (for enantiomeric excess determinations). HPLC analyses were carried out with a Hewlett Packard series 1100 apparatus equipped with 250 mm × 4.6 mm Daicel Chiralcel® AD or OD analytical columns.

**General Procedure for Palladium-Catalysed Allylic Alkylation with Dimethyl Malonate:** A mixture of the diphospholane ligand (12 μmol) and [Pd(η<sup>3</sup>-C<sub>3</sub>H<sub>5</sub>)Cl]<sub>2</sub> (1.8 mg, 5 μmol) in the appropriate solvent (CH<sub>2</sub>Cl<sub>2</sub> or THF, 2 mL) was stirred at room temperature for 20 min. When BSA was used as a base, a suspension of KOAc (1 mg, 10 μmol) in the solvent (1 mL) was added to the catalyst solution, followed by a mixture of dimethyl malonate (264 mg, 2 mmol) and BSA (407 mg, 2 mmol) in the solvent (4 mL) and a solution of the substrate (1 mmol) in the solvent (1 mL). When NaH was used as a base, a solution of dimethyl sodiomalonate was prepared by allowing a solution of dimethyl malonate (264 mg, 2 mmol) in THF (1 mL) to react with a suspension of NaH (48 mg, 2 mmol) in THF (4 mL). A solution of the substrate (1 mmol) in THF (1 mL) was added to the catalyst solution, followed by the nucleophile solution. In both cases, the conversion was periodically monitored by GC. When the reaction was complete, water (25 mL) was added, and the organic phase was extracted with Et<sub>2</sub>O (3 × 30 mL). The extract was dried with MgSO<sub>4</sub> and the solvent was removed under reduced pressure. The crude product was purified by column chromatography on silica gel with pentane/Et<sub>2</sub>O (4:1, v/v). By comparison with literature data, the alkylation products were identified and, if necessary, their absolute stereochemistry was determined by polarimetry: dimethyl (*E*)-(1,3-diphenylprop-2-en-1-yl-

malonate (**4a**),<sup>[34]</sup> dimethyl (*E*)-(pent-3-en-2-yl)malonate (**4b**),<sup>[35]</sup> dimethyl (cyclohex-2-en-1-yl)malonate (**4c**) and dimethyl (cyclopent-2-en-1-yl)malonate (**4d**),<sup>[36]</sup> dimethyl (*E*)-(4-phenylbut-3-en-2-yl)malonate (**6a**) and dimethyl (*E*)-(1-phenylbut-2-en-1-yl)malonate (**7a**),<sup>[8,9]</sup> dimethyl (*E*)-(5-methylhex-3-en-2-yl)malonate (**6b**) and dimethyl (*E*)-(2-methylhex-4-en-3-yl)malonate (**7b**).<sup>[35]</sup> The *ee* values were measured with the following methods: **4a**, chiral HPLC (Chiralcel AD, 1 mL·min<sup>-1</sup>; eluent *n*-hexane/*i*PrOH, 95:5, v/v); **4b** and **4c**, chiral GC; **4d**, **6a**, **7a**, **6b**, and **7b**, <sup>1</sup>H NMR in CDCl<sub>3</sub> using Eu(hfc)<sub>3</sub> as a chiral shift reagent.

**General Procedure for Palladium-Catalysed Allylic Alkylation with 2-Methyl-1-Tetralone:** The procedure was adapted from ref.<sup>[13]</sup> To a solution or suspension of base (1.85 mmol) in THF (2 mL) was added 2-methyl-1-tetralone (150 mg, 0.94 mmol). A mixture of ligand **2** (4.4 mg, 10 μmol) and [Pd(η<sup>3</sup>-C<sub>3</sub>H<sub>5</sub>)Cl]<sub>2</sub> (1.8 mg, 5 μmol) in THF (1 mL) was stirred at room temperature for 20 min. To the catalyst solution was added allyl acetate (187 mg, 1.87 mmol), followed by the nucleophile solution. The conversion was periodically monitored by GC. When the reaction was complete, the mixture was added to a 0.2 M aqueous HCl solution (25 mL) and extracted with Et<sub>2</sub>O (3 × 30 mL). The extract was treated with saturated NaHCO<sub>3</sub> (aq.) and dried with MgSO<sub>4</sub>. The solvent was removed under reduced pressure and the crude 2-allyl-2-methyl-1-tetralone purified by column chromatography on silica gel with pentane/EtOAc (v/v, 9:1; R<sub>f</sub> = 0.52). The *ee* of the product was determined by chiral HPLC (Chiralcel OD, 0.7 mL·min<sup>-1</sup>; eluent *n*-hexane/*i*PrOH, 99.9:0.1, v/v) and its absolute stereochemistry was assigned by comparison with ref.<sup>[13]</sup>

**General Procedure for the Heck Reaction:** The procedure was adapted from ref.<sup>[14]</sup> A mixture of diphospholane ligand (24 μmol) and the Pd source (12 μmol) in benzene (2 mL) was stirred at room temperature for 20 min. To the catalyst solution were successively added a solution of PhOTf (89 mg, 0.394 mmol) in benzene (1 mL), NiPr<sub>2</sub>Et (168 mg, 1.30 mmol), 2,3-dihydrofuran (155 mg, 2.21 mmol) and additional benzene (2 mL). The mixture was heated to reflux for 48 h. The solvent was removed under reduced pressure and the crude products were purified by column chromatography on silica gel with pentane/EtOAc (9:1, v/v). The absolute stereochemistry of the product was determined by comparing the sign of its optical rotation with data from ref.<sup>[14]</sup> The *ee* values were measured by chiral GC.

**[Pd((*S,S*)-Duphos)(η<sup>3</sup>-cyclohexenyl)](BF<sub>4</sub>) (**10**):** To a solution of [Pd(η<sup>3</sup>-C<sub>6</sub>H<sub>9</sub>)Cl]<sub>2</sub> (35 mg, 0.078 mmol) in acetonitrile (4 mL) was added dropwise in the dark at room temperature a solution of AgBF<sub>4</sub> (35 mg, 0.180 mmol) in acetonitrile (3 mL). After 10 min of stirring, the suspension was filtered through Celite and a suspension of (*S,S*)-Duphos (48 mg, 0.157 mmol) in acetonitrile (1 mL) was added to the colourless filtrate. A pale orange solution was obtained after 30 min of stirring. The solvent was evaporated in vacuo to afford a brown powder which was washed with diethyl ether. The product was recrystallized from dichloromethane/pentane as colourless crystals. Yield: 50 mg (55%). <sup>31</sup>P{<sup>1</sup>H} NMR (CD<sub>2</sub>Cl<sub>2</sub>, 121 MHz): δ = 68.2 (d, <sup>2</sup>J<sub>P,P</sub> = 36 Hz, 1 P), 71.9 (d, <sup>2</sup>J<sub>P,P</sub> = 36 Hz, 1 P) ppm. <sup>1</sup>H NMR (CD<sub>3</sub>CN, 300 MHz): δ 0.62 (dd, <sup>3</sup>J<sub>H,H</sub> = 7.0, <sup>3</sup>J<sub>H,P</sub> = 15.6 Hz, 3 H, CH<sub>3</sub>), 0.85 (dd, <sup>3</sup>J<sub>H,H</sub> = 7.0, <sup>3</sup>J<sub>H,P</sub> = 15.6 Hz, 3 H, CH<sub>3</sub>), 1.12 (dd, <sup>3</sup>J<sub>H,H</sub> = 7.0, <sup>3</sup>J<sub>H,P</sub> = 20.8 Hz, 3 H, CH<sub>3</sub>), 1.35 (dd, <sup>3</sup>J<sub>H,H</sub> = 7.1, <sup>3</sup>J<sub>H,P</sub> = 20.5 Hz, 3 H, CH<sub>3</sub>), 1.60–3.20 (m, 18 H, CH + CH<sub>2</sub>), 5.33 (t, <sup>3</sup>J<sub>H,H</sub> = 7.1 Hz, 1 H, H<sup>2</sup>), 5.90 (m, 2 H, H<sup>1</sup> + H<sup>3</sup>), 7.60–7.90 (m, 4 H, H<sub>ar</sub>) ppm. <sup>13</sup>C{<sup>1</sup>H} NMR (CD<sub>2</sub>Cl<sub>2</sub>, 75 MHz): δ = 14.8 (s, 2 CH<sub>3</sub>), 18.4 (d, <sup>2</sup>J<sub>C,P</sub> = 12 Hz, CH<sub>3</sub>), 18.7 (d, <sup>2</sup>J<sub>C,P</sub> = 12 Hz, CH<sub>3</sub>), 20.4 (s, CH<sub>2</sub>), 28.1 (d, <sup>2</sup>J<sub>C,P</sub> = 5 Hz, CH<sub>2</sub>), 29.4 (d, <sup>2</sup>J<sub>C,P</sub> = 5 Hz, CH<sub>2</sub>), 36.2 (d,

$^2J_{C,P} = 5$  Hz, CH<sub>2</sub>), 36.5 (d,  $^2J_{C,P} = 5$  Hz, CH<sub>2</sub>), 37.2 (s, CH<sub>2</sub>), 37.5 (s, CH<sub>2</sub>), 38.6 (d,  $^1J_{C,P} = 24$  Hz, CH), 40.7 (d,  $^1J_{C,P} = 22$  Hz, CH), 41.0 (d,  $^1J_{C,P} = 26$  Hz, CH), 41.3 (d,  $^1J_{C,P} = 24$  Hz, CH), 81.9 (dd,  $^2J_{C,P} = 29$ ,  $^2J_{C,P} = 3$  Hz, C<sub>allyl</sub> terminal), 87.1 (dd,  $^2J_{C,P} = 29$ ,  $^2J_{C,P} = 3$  Hz, C<sub>allyl</sub> terminal), 113.8 (t,  $^2J_{C,P} = 7$  Hz, C<sub>allyl</sub> central), 132.6 (s, 2 CH<sub>ar</sub>), 134.1 (d,  $^2J_{C,P} = 12$  Hz, CH<sub>ar</sub>), 134.3 (d,  $^2J_{C,P} = 12$  Hz, CH<sub>ar</sub>), 141.2 (m, 2 C<sub>ar</sub>) ppm. MS (FAB<sup>+</sup>, NBA matrix):  $m/z$  (%) = 493.0 (100) [M - BF<sub>4</sub>]<sup>+</sup>, 412.9 (37) [M + 1 - BF<sub>4</sub> - C<sub>6</sub>H<sub>9</sub>]<sup>+</sup>. C<sub>24</sub>H<sub>37</sub>BF<sub>4</sub>P<sub>2</sub>Pd (580.71): calcd. C 49.64, H 6.42, P 10.67; found C 49.59, H 6.34, P 10.80.

**[Pd{(R,R)-Duxantphos}(η<sup>3</sup>-cyclohexenyl)](SbF<sub>6</sub>) (11):** To a solution of [Pd(η<sup>3</sup>-C<sub>6</sub>H<sub>9</sub>)Cl]<sub>2</sub> (20 mg, 0.045 mmol) in THF (2 mL) was added dropwise in the dark at room temperature a solution of AgSbF<sub>6</sub> (32 mg, 0.093 mmol) in THF (2 mL). After 15 min of stirring, the suspension was filtered through Celite and a solution of (R,R)-Duxantphos (42 mg, 0.096 mmol) in THF (2 mL) was added to the colourless filtrate. A yellow solution was obtained after 30 min of stirring and the solvent was evaporated in vacuo to afford a yellow powder which was washed with pentane. The product was recrystallized from dichloromethane/diethyl ether. Yield: 72 mg (93%). <sup>31</sup>P{<sup>1</sup>H} NMR (CD<sub>2</sub>Cl<sub>2</sub>, 121 MHz): δ = 33.7 (d,  $^2J_{P,P} = 41$  Hz, 1 P), 35.5 (d,  $^2J_{P,P} = 41$  Hz, 1 P) ppm. <sup>1</sup>H NMR (CD<sub>2</sub>Cl<sub>2</sub>, 300 MHz): δ = 0.06 (m, 1 H, CH<sub>2</sub>), 0.24 (m, 1 H, CH<sub>2</sub>), 0.46 (m, 1 H, CH<sub>2</sub>), 0.60–0.80 (m, 2 H, CH<sub>2</sub>), 1.13 (dd,  $^3J_{H,H} = 7.3$ ,  $^3J_{H,P} = 14.7$  Hz, 3 H, CH<sub>3</sub> phospholane), 1.25 (dd,  $^3J_{H,H} = 7.6$ ,  $^3J_{H,P} = 20.5$  Hz, 3 H, CH<sub>3</sub> phospholane), 1.32 (dd,  $^3J_{H,H} = 7.6$ ,  $^3J_{H,P} = 19.3$  Hz, 3 H, CH<sub>3</sub> phospholane), 1.20–1.75 (m, 3 H, CH<sub>2</sub>), 1.41 (s, 3 H, CH<sub>3</sub> xanthene), 1.79 (s, 3 H, CH<sub>3</sub> xanthene), 1.80 (dd,  $^3J_{H,H} = 7.3$ ,  $^3J_{H,P} = 14.2$  Hz, 3 H, CH<sub>3</sub> phospholane), 2.07–2.40 (m, 5 H, CH<sub>2</sub>), 2.63 (m, 1 H, CH<sub>2</sub>), 2.80–3.00 (m, 3 H, CH), 3.09 (m, 1 H, CH), 5.20 (t,  $^3J_{H,H} = 7.1$  Hz, 1 H, H<sup>2</sup>), 5.60–5.75 (m, 2 H, H<sup>1</sup> + H<sup>3</sup>), 7.13–7.30 (m, 2 H, H<sub>ar</sub>), 7.36 (m, 1 H, H<sub>ar</sub>), 7.50–7.62 (m, 3 H, H<sub>ar</sub>) ppm. <sup>13</sup>C{<sup>1</sup>H} NMR (CD<sub>3</sub>CN, 75 MHz): δ = 14.5 (s, CH<sub>3</sub> phospholane), 17.5 (d,  $^2J_{C,P} = 5$  Hz, CH<sub>3</sub> phospholane), 19.4 (d,  $^2J_{C,P} = 9$  Hz, CH<sub>3</sub> phospholane), 20.0 (s, CH<sub>2</sub>), 20.2 (d,  $^2J_{C,P} = 14$  Hz, CH<sub>3</sub> phospholane), 24.2 (s, CH<sub>3</sub> xanthene), 26.9 (d,  $^2J_{C,P} = 5$  Hz, CH<sub>2</sub>), 27.2 (d,  $^2J_{C,P} = 5$  Hz, CH<sub>2</sub>), 32.1 (s, CH<sub>2</sub>), 32.4 (s, CH<sub>3</sub> xanthene), 32.6 (s, CH<sub>2</sub>), 32.9 (d,  $^1J_{C,P} = 22$  Hz, CH), 33.6 (s, CH<sub>2</sub>), 33.9 (d,  $^1J_{C,P} = 20$  Hz, CH), 34.0 (d,  $^1J_{C,P} = 14$  Hz, CH), 34.7 (s, CH<sub>2</sub>), 36.8 [s, C(CH<sub>3</sub>)<sub>2</sub>], 37.0 (d,  $^1J_{C,P} = 27$  Hz, CH), 81.3 (d,  $^2J_{C,P} = 28$  Hz, C<sub>allyl</sub> terminal), 93.3 (d,  $^2J_{C,P} = 25$  Hz, C<sub>allyl</sub> terminal), 109.1 (t,  $^2J_{C,P} = 5$  Hz, C<sub>allyl</sub> central), 119.2 (d,  $^2J_{C,P} = 27$  Hz, C<sub>ar</sub>), 120.1 (d,  $^2J_{C,P} = 23$  Hz, C<sub>ar</sub>), 125.4 (d,  $^3J_{C,P} = 4$  Hz, CH<sub>ar</sub>), 126.2 (d,  $^3J_{C,P} = 4$  Hz, CH<sub>ar</sub>), 128.3 (s, CH<sub>ar</sub>), 128.8 (s, 2 CH<sub>ar</sub>), 130.9 (s, CH<sub>ar</sub>), 134.4 (s, C<sub>ar</sub>), 135.2 (s, C<sub>ar</sub>), 153.4 (d,  $^1J_{C,P} = 7$  Hz, C<sub>ar</sub>), 153.8 (d,  $^1J_{C,P} = 7$  Hz, C<sub>ar</sub>) ppm. MS (FAB<sup>+</sup>, NBA matrix):  $m/z$  (%) = 625.2 (68) [M - SbF<sub>6</sub>]<sup>+</sup>, 545.1 (100) [M + 1 - SbF<sub>6</sub> - C<sub>6</sub>H<sub>9</sub>]<sup>+</sup>.

**[Pd{(R,R)-Duxantphos}(η<sup>3</sup>-1,3-diphenylallyl)](SbF<sub>6</sub>) (12):** To a suspension of [Pd(η<sup>3</sup>-Ph<sub>2</sub>C<sub>3</sub>H<sub>3</sub>)Cl]<sub>2</sub> (30 mg, 0.045 mmol) in CH<sub>2</sub>Cl<sub>2</sub> (3 mL) was added dropwise in the dark at room temperature a solution of AgSbF<sub>6</sub> (31 mg, 0.090 mmol) in CH<sub>2</sub>Cl<sub>2</sub> (2 mL). After 20 min of stirring, the suspension was filtered through Celite and a solution of (R,R)-Duxantphos (40 mg, 0.091 mmol) in CH<sub>2</sub>Cl<sub>2</sub> (2 mL) was added to the red filtrate. An orange-brown solution was obtained after 20 min of stirring. The product precipitated upon slow addition of pentane. It was then separated from the yellow supernatant, washed with diethyl ether, and dried. Yield: 70 mg (80%). HRMS (FAB<sup>+</sup>, NBA matrix):  $m/z$  calcd. for C<sub>42</sub>H<sub>49</sub>OP<sub>2</sub><sup>105</sup>Pd 736.23094; found 736.23067.

**syn,syn,exo-12a:** <sup>31</sup>P{<sup>1</sup>H} NMR (CD<sub>2</sub>Cl<sub>2</sub>, 202.5 MHz, 193 K): δ = 27.6 (d,  $^2J_{P,P} = 52$  Hz, 1 P), 39.2 (d,  $^2J_{P,P} = 52$  Hz, 1 P) ppm. <sup>1</sup>H NMR (CD<sub>2</sub>Cl<sub>2</sub>, 500 MHz, 193 K), selected data (see also

Scheme 3): δ = -0.08 (dd,  $^3J_{H,H} = 7.0$ ,  $^3J_{H,P} = 14.9$  Hz, 3 H, CH<sub>3</sub> phospholane), 0.85 (dd,  $^3J_{H,H} = 7.4$ ,  $^3J_{H,P} = 22.2$  Hz, 3 H, CH<sub>3</sub> phospholane), 0.87 (dd,  $^3J_{H,H} = 7.1$ ,  $^3J_{H,P} = 14.0$  Hz, 3 H, CH<sub>3</sub> phospholane), 1.05 (dd,  $^3J_{H,H} = 7.4$ ,  $^3J_{H,P} = 22.2$  Hz, 3 H, CH<sub>3</sub> phospholane), 1.58 (s, 3 H, CH<sub>3</sub> xanthene), 1.65 (s, 3 H, CH<sub>3</sub> xanthene), 4.69 (t,  $^3J_{H,H} = ^3J_{H,P} = 10.8$  Hz, 1 H, H<sub>allyl</sub>), 5.38 (dd,  $^3J_{H,H} = 13.7$ ,  $^3J_{H,P} = 9.4$  Hz, 1 H, H<sub>allyl</sub>), 6.35 (ddd,  $^3J_{H,H} = 14.0$ ,  $^3J_{H,H} = 10.0$ ,  $^3J_{H,P} = 2.2$  Hz, 1 H, H<sub>allyl</sub>) ppm. <sup>13</sup>C{<sup>1</sup>H} NMR (CD<sub>3</sub>NO<sub>2</sub>, 125 MHz, 263 K), selected data: δ = 14.6 (s, CH<sub>3</sub> phospholane), 15.2 (s, 2 CH<sub>3</sub> phospholane), 17.8 (s, CH<sub>3</sub> phospholane), 21.3 (d,  $^1J_{C,P} = 14$  Hz, CH), 22.5 (d,  $^1J_{C,P} = 13$  Hz, CH), 25.0 (s, CH<sub>3</sub> xanthene), 29.2 (s, CH<sub>3</sub> xanthene), 33.2 (s, CH<sub>2</sub>), 34.9 (s, CH<sub>2</sub>), 35.1 (s, CH<sub>2</sub>), 36.3 (s, CH<sub>2</sub>), 36.7 (d,  $^1J_{C,P} = 20$  Hz, CH), 38.2 (d,  $^1J_{C,P} = 19$  Hz, CH), 38.6 [s, C(CH<sub>3</sub>)<sub>2</sub>], 77.8 (d,  $^2J_{C,P} = 30$  Hz, C<sub>allyl</sub> terminal), 100.2 (d,  $^2J_{C,P} = 20$  Hz, C<sub>allyl</sub> terminal), 110.4 (s, C<sub>allyl</sub> central) ppm.

**syn,syn,endo-12b:** <sup>31</sup>P{<sup>1</sup>H} NMR (CD<sub>2</sub>Cl<sub>2</sub>, 202.5 MHz, 193 K): δ = 32.8 (d,  $^2J_{P,P} = 57$  Hz, 1 P), 40.6 (d,  $^2J_{P,P} = 57$  Hz, 1 P) ppm. <sup>1</sup>H NMR (CD<sub>2</sub>Cl<sub>2</sub>, 500 MHz, 193 K), selected data (see also Scheme 3): δ = 0.80 (dd,  $^3J_{H,H} = 7.2$ ,  $^3J_{H,P} = 14.5$  Hz, 3 H, CH<sub>3</sub> phospholane), 0.96 (dd,  $^3J_{H,H} = 7.4$ ,  $^3J_{H,P} = 15.1$  Hz, 3 H, CH<sub>3</sub> phospholane), 1.10 (dd,  $^3J_{H,H} = 7.6$ ,  $^3J_{H,P} = 22.4$  Hz, 3 H, CH<sub>3</sub> phospholane), 1.32 (s, 3 H, CH<sub>3</sub> xanthene), 1.36 (dd,  $^3J_{H,H} = 7.3$ ,  $^3J_{H,P} = 18.8$  Hz, 3 H, CH<sub>3</sub> phospholane), 1.88 (s, 3 H, CH<sub>3</sub> xanthene), 4.92 (t,  $^3J_{H,H} = ^3J_{H,P} = 11.1$  Hz, 1 H, H<sub>allyl</sub>), 5.03 (dd,  $^3J_{H,H} = 13.0$ ,  $^3J_{H,P} = 9.2$  Hz, 1 H, H<sub>allyl</sub>), 5.21 (t,  $^3J_{H,H} = 12.5$  Hz, 1 H, H<sub>allyl</sub>) ppm.

**Minor Isomer 12c:** <sup>31</sup>P{<sup>1</sup>H} NMR (CD<sub>2</sub>Cl<sub>2</sub>, 202.5 MHz, 193 K): δ = 35.3 (d,  $^2J_{P,P} = 45$  Hz, 1 P), 37.2 (d,  $^2J_{P,P} = 45$  Hz, 1 P) ppm.

**Minor Isomer 12d:** <sup>31</sup>P{<sup>1</sup>H} NMR (CD<sub>2</sub>Cl<sub>2</sub>, 202.5 MHz, 193 K): δ = 28.3 (d,  $^2J_{P,P} = 46$  Hz, 1 P), 36.0 (d,  $^2J_{P,P} = 46$  Hz, 1 P) ppm.

**[Pd{(R,R)-Duxantphos}(η<sup>3</sup>-allyl)](SbF<sub>6</sub>) (13):** To a solution of [Pd(η<sup>3</sup>-C<sub>3</sub>H<sub>5</sub>)Cl]<sub>2</sub> (35 mg, 0.096 mmol) in CH<sub>2</sub>Cl<sub>2</sub> (4 mL) was added dropwise in the dark at room temperature a solution of AgSbF<sub>6</sub> (63 mg, 0.183 mmol) in CH<sub>2</sub>Cl<sub>2</sub> (1 mL). After 10 min of stirring, the suspension was filtered through Celite and a solution of (R,R)-Duxantphos (80 mg, 0.182 mmol) in CH<sub>2</sub>Cl<sub>2</sub> (2 mL) was added to the yellow filtrate. A brown solution was obtained after 10 min of stirring. The volume was reduced in vacuo and the product was precipitated by slow addition of pentane and collected on a frit as a brown powder. Yield: 115 mg (77%). <sup>31</sup>P{<sup>1</sup>H} NMR (CD<sub>2</sub>Cl<sub>2</sub>, 121 MHz): δ = 33.1 (d,  $^2J_{P,P} = 38$  Hz, 1 P), 33.5 (d,  $^2J_{P,P} = 38$  Hz, 1 P) ppm. <sup>1</sup>H NMR (CD<sub>2</sub>Cl<sub>2</sub>, 500 MHz), selected data (see also Scheme 6): δ = 1.21 (dd,  $^3J_{H,H} = 7.3$ ,  $^3J_{H,P} = 14.6$  Hz, 3 H, CH<sub>3</sub> phospholane), 1.33 (dd,  $^3J_{H,H} = 7.5$ ,  $^3J_{H,P} = 20.2$  Hz, 3 H, CH<sub>3</sub> phospholane), 1.36 (dd,  $^3J_{H,H} = 7.5$ ,  $^3J_{H,P} = 19.5$  Hz, 3 H, CH<sub>3</sub> phospholane), 1.52 (dd,  $^3J_{H,H} = 7.2$ ,  $^3J_{H,P} = 14.5$  Hz, 3 H, CH<sub>3</sub> phospholane), 1.52 (s, 3 H, CH<sub>3</sub> xanthene), 1.68 (s, 3 H, CH<sub>3</sub> xanthene), 1.60–2.10 (m, 4 H, CH<sub>2</sub>), 2.20–2.40 (m, 3 H, CH<sub>2</sub>), 2.51 (m, 1 H, CH<sub>2</sub>), 2.55 (dd,  $^3J_{H,H} = 13.6$ ,  $^3J_{H,P} = 8.8$  Hz, 1 H, H<sub>anti</sub>), 2.73 (dd,  $^3J_{H,H} = 13.1$ ,  $^3J_{H,P} = 9.6$  Hz, 1 H, H<sub>anti</sub>), 2.85–3.10 (m, 4 H, CH), 4.51 (dddd,  $^3J_{H,H} = 7.4$ ,  $^4J_{H,H} = 2.3$ ,  $^3J_{H,P} = 2.2$ , 0.6 Hz, 1 H, H<sub>syn</sub>), 4.66 (dddd,  $^3J_{H,H} = 7.2$ ,  $^4J_{H,H} = 2.5$ ,  $^3J_{H,P} = 2.9$ , 0.6 Hz, 1 H, H<sub>syn</sub>), 5.18 (tt,  $^3J_{H,H} = 13.3$ ,  $^3J_{H,H} = 7.3$  Hz, 1 H, H<sub>central</sub>), 7.28 (td,  $^3J_{H,H} = 7.7$ ,  $^4J_{H,P} = 1.5$  Hz, 1 H, H<sub>ar</sub>), 7.31 (td,  $^3J_{H,H} = 7.6$ ,  $^4J_{H,P} = 1.5$  Hz, 1 H, H<sub>ar</sub>), 7.37 (ddd,  $^3J_{H,H} = 7.7$ ,  $^4J_{H,H} = 1.4$ ,  $^3J_{H,P} = 6.3$  Hz, 1 H, H<sub>ar</sub>), 7.46 (ddd,  $^3J_{H,H} = 7.7$ ,  $^4J_{H,H} = 1.2$ ,  $^3J_{H,P} = 7.6$  Hz, 1 H, H<sub>ar</sub>), 7.57 (ddd,  $^3J_{H,H} = 7.7$ ,  $^4J_{H,H} = 1.3$ ,  $^3J_{H,P} = 0.8$  Hz, 1 H, H<sub>ar</sub>), 7.59 (ddd,  $^3J_{H,H} = 7.8$ ,  $^4J_{H,H} = 1.4$ ,  $^3J_{H,P} = 0.7$  Hz, 1 H, H<sub>ar</sub>) ppm. <sup>13</sup>C{<sup>1</sup>H} NMR (CD<sub>2</sub>Cl<sub>2</sub>, 100 MHz): δ = 14.9 (d,  $^2J_{C,P} = 2$  Hz, CH<sub>3</sub> phospholane), 15.9 (d,  $^2J_{C,P} = 4$  Hz, CH<sub>3</sub> phospholane), 19.3

Table 5. Crystal and refinement data for compounds **10** and **11**

	<b>10</b>	<b>11</b>
Empirical formula	C <sub>24</sub> H <sub>37</sub> P <sub>2</sub> Pd·BF <sub>4</sub>	C <sub>33</sub> H <sub>45</sub> OP <sub>2</sub> Pd·SbF <sub>6</sub>
Formula mass	580.72	861.81
Colour	colourless	colourless
Crystal system	monoclinic	orthorhombic
<i>a</i> [Å]	8.2100(2)	12.041(1)
<i>b</i> [Å]	18.6150(7)	12.425(2)
<i>c</i> [Å]	8.5920(3)	22.917(4)
β [°]	97.553(2)	90
<i>V</i> [Å <sup>3</sup> ]	1301.7(1)	3428(1)
<i>Z</i>	2	4
<i>D</i> <sub>calcd.</sub> [g cm <sup>-3</sup> ]	1.48	1.67
<i>F</i> 000	596	1728
Wavelength [Å]	0.71073	0.71073
μ [mm <sup>-1</sup> ]	0.874	1.459
Space group	P 1 2 <sub>1</sub> 1	P 2 <sub>1</sub> 2 <sub>1</sub> 2 <sub>1</sub>
Diffractionmeter	KappaCCD	MACH3 Nonius
Cryst dimens [mm]	0.15 × 0.12 × 0.12	0.40 × 0.25 × 0.20
Temperature [K]	173	173
Radiation	Mo- <i>K</i> <sub>α</sub> graphite-monochromated	Mo- <i>K</i> <sub>α</sub> graphite-monochromated
Scan mode	φ scans	0/20
<i>hkl</i> limits	-10/10, -26/26, -12/12	0/15, -15/0, 0/28
θ limits [°]	2.5/30.56	2.5/26.29
No. of data measured	19463	3917
No. of data with <i>I</i> > 3σ( <i>I</i> )	2887	3318
Weighting scheme	4 <i>F</i> <sub>o</sub> <sup>2</sup> /[σ <sup>2</sup> ( <i>F</i> <sub>o</sub> <sup>2</sup> ) + 0.0004 <i>F</i> <sub>o</sub> <sup>4</sup> ] + 1.0	4 <i>F</i> <sub>o</sub> <sup>2</sup> /[σ <sup>2</sup> ( <i>F</i> <sub>o</sub> <sup>2</sup> ) + 0.0016 <i>F</i> <sub>o</sub> <sup>4</sup> ]
No. of variables	297	397
<i>R</i>	0.067	0.025
<i>R</i> <sub>w</sub>	0.088	0.031
Flack parameter	0.0(1)	-0.02(3)
Largest peak in final difference [e·Å <sup>-3</sup> ]	0.738	0.567
GOF	1.612	1.096

(d, <sup>2</sup>*J*<sub>C,P</sub> = 9 Hz, CH<sub>3</sub> phospholane), 19.9 (d, *J*<sub>C,P</sub> = 10 Hz, CH<sub>3</sub> phospholane), 25.9 (s, CH<sub>3</sub> xanthene), 29.4 (s, CH<sub>3</sub> xanthene), 32.0 (s, CH<sub>2</sub>), 32.4 (s, CH<sub>2</sub>), 32.7 (s, CH<sub>2</sub>), 33.3 (s, CH<sub>2</sub>), 33.4 (dd, <sup>1</sup>*J*<sub>C,P</sub> = 23, <sup>3</sup>*J*<sub>C,P</sub> = 2 Hz, CH), 33.7 (dd, <sup>1</sup>*J*<sub>C,P</sub> = 17, <sup>3</sup>*J*<sub>C,P</sub> = 2 Hz, CH), 34.0 (dd, <sup>1</sup>*J*<sub>C,P</sub> = 19, <sup>3</sup>*J*<sub>C,P</sub> = 3 Hz, CH), 35.3 (dd, <sup>1</sup>*J*<sub>C,P</sub> = 22, <sup>3</sup>*J*<sub>C,P</sub> = 3 Hz, CH), 36.1 [s, C(CH<sub>3</sub>)<sub>2</sub>], 66.8 (dd, <sup>2</sup>*J*<sub>C,P</sub> = 26, <sup>2</sup>*J*<sub>C,P</sub> = 3 Hz, CH<sub>allyl</sub> terminal), 72.6 (dd, <sup>2</sup>*J*<sub>C,P</sub> = 25, <sup>2</sup>*J*<sub>C,P</sub> = 3 Hz, CH<sub>allyl</sub> terminal), 118.2 (dd, <sup>2</sup>*J*<sub>C,P</sub> = 27, <sup>4</sup>*J*<sub>C,P</sub> = 2 Hz, C<sub>ar</sub>), 118.5 (dd, <sup>2</sup>*J*<sub>C,P</sub> = 24, <sup>4</sup>*J*<sub>C,P</sub> = 2 Hz, C<sub>ar</sub>), 118.7 (t, <sup>2</sup>*J*<sub>C,P</sub> = 5 Hz, CH<sub>allyl</sub> central), 124.8 (d, <sup>2</sup>*J*<sub>C,P</sub> = 6 Hz, CH<sub>ar</sub>), 125.3 (d, <sup>2</sup>*J*<sub>C,P</sub> = 5 Hz, CH<sub>ar</sub>), 127.3 (s, CH<sub>ar</sub>), 127.6 (d, <sup>3</sup>*J*<sub>C,P</sub> = 2 Hz, CH<sub>ar</sub>), 127.9 (d, <sup>3</sup>*J*<sub>C,P</sub> = 2 Hz, CH<sub>ar</sub>), 128.6 (s, CH<sub>ar</sub>), 134.1 (d, <sup>3</sup>*J*<sub>C,P</sub> = 3 Hz, C<sub>ar</sub>), 134.4 (d, <sup>3</sup>*J*<sub>C,P</sub> = 3 Hz, C<sub>ar</sub>), 153.2 (d, <sup>1</sup>*J*<sub>C,P</sub> = 6 Hz, C<sub>ar</sub>), 153.4 (d, <sup>1</sup>*J*<sub>C,P</sub> = 6 Hz, C<sub>ar</sub>) ppm. HRMS (FAB<sup>+</sup>, NBA matrix): *m/z* calcd. for C<sub>30</sub>H<sub>41</sub>OP<sub>2</sub><sup>105</sup>Pd 584.1683; found 584.1689.

**X-ray Crystallographic Studies:** Details of data collection parameters and refinement results are listed in Table 5. The structures were solved by direct methods. Hydrogen atoms were introduced as fixed contributors in calculated positions [C–H = 0.95 Å, *B*(H) = 1.3 *B*<sub>equiv</sub>]. Final difference maps revealed no significant maxima. All calculations were performed using the Nonius OpenMoleN package.<sup>[37]</sup> Neutral atom scattering factor coefficients and anomalous dispersion coefficients were taken from a standard source.<sup>[38]</sup> CCDC-236309 (**10**) and -236310 (**11**) contain the supplementary crystallographic data for this paper. These data can be obtained free of charge at [www.ccdc.cam.ac.uk/conts/retrieving.html](http://www.ccdc.cam.ac.uk/conts/retrieving.html) [or from the Cambridge Crystallography Data Centre, 12 Union Road, Cambridge CB2 1EZ, UK [Fax: + 44-1223/336-033; E-mail: [deposit@ccdc.cam.ac.uk](mailto:deposit@ccdc.cam.ac.uk)]].

## Acknowledgments

We thank Denis Sinou for helpful discussions and Rafael Aguado and Peter Dierkes for a gift of ligand **2**. Financial support from the Centre National de la Recherche Scientifique is gratefully acknowledged.

- [1] Reviews and selected papers: <sup>[1a]</sup> C. G. Frost, J. Howarth, J. M. J. Williams, *Tetrahedron: Asymmetry* **1992**, *3*, 1089–1122. <sup>[1b]</sup> B. M. Trost, D. L. Van Vranken, *Chem. Rev.* **1996**, *96*, 395–422. <sup>[1c]</sup> G. Helmchen, *J. Organomet. Chem.* **1999**, *576*, 203–214. <sup>[1d]</sup> K. H. Ahn, C.-W. Cho, J. Park, S. Lee, *Tetrahedron: Asymmetry* **1997**, *8*, 1179–1185. <sup>[1e]</sup> A. Saitoh, M. Misawa, T. Morimoto, *Tetrahedron: Asymmetry* **1999**, *10*, 1025–1028. <sup>[1f]</sup> W. Zhang, T. Shimanuki, T. Kida, Y. Nakatsuji, I. Ikeda, *J. Org. Chem.* **1999**, *64*, 6247–6251. <sup>[1g]</sup> D. A. Evans, K. R. Campos, J. D. Tedrow, F. E. Michael, M. R. Gagné, *J. Am. Chem. Soc.* **2000**, *122*, 7905–7920. <sup>[1h]</sup> K. Ito, R. Kashiwagi, S. Hayashi, T. Uchida, T. Katsuki, *Synlett* **2001**, 284–286. <sup>[1i]</sup> S. J. Greenfield, A. Agarkov, S. R. Gilbertson, *Org. Lett.* **2003**, *5*, 3069–3072.
- [2] <sup>[2a]</sup> A. Pfaltz, M. Lautens, in: *Comprehensive Asymmetric Catalysis* (Eds.: E. Jacobsen, A. Pfaltz, H. Yamamoto), Springer, Berlin, **1999**, vol. II, chapter 24, pp. 833–884. <sup>[2b]</sup> M. Shibasaki, E. M. Vogl, in: *Comprehensive Asymmetric Catalysis* (Eds.: E. Jacobsen, A. Pfaltz, H. Yamamoto), Springer, Berlin, **1999**, vol. I, chapter 14, pp. 457–487.
- [3] <sup>[3a]</sup> P. S. Pregosin, G. Trabesinger, *J. Chem. Soc., Dalton Trans.* **1998**, 727–734. <sup>[3b]</sup> P. S. Pregosin, R. Salzmann, *Coord. Chem. Rev.* **1996**, *155*, 35–68.

- [4] [4a] P. Dierkes, S. Ramdeehul, L. Barloy, A. De Cian, J. Fischer, P. C. J. Kamer, P. W. N. M. van Leeuwen, J. A. Osborn, *Angew. Chem. Int. Ed.* **1998**, *37*, 3116–3118. [4b] S. Ramdeehul, P. Dierkes, R. Aguado, P. C. J. Kamer, P. W. N. M. van Leeuwen, J. A. Osborn, *Angew. Chem. Int. Ed.* **1998**, *37*, 3118–3121.
- [5] M. J. Burk, *Acc. Chem. Res.* **2000**, *33*, 363–372.
- [6] [6a] P. Dierkes, P. W. N. M. van Leeuwen, *J. Chem. Soc., Dalton Trans.* **1999**, 1519–1529. [6b] P. W. N. M. van Leeuwen, P. C. J. Kamer, J. N. H. Reek, P. Dierkes, *Chem. Rev.* **2000**, *100*, 2741–2769. [6c] Z. Freixa, P. W. N. M. van Leeuwen, *Dalton Trans.* **2003**, 1890–1901.
- [7] D. Drago, P. S. Pregosin, *J. Chem. Soc., Dalton Trans.* **2000**, 3191–3196.
- [8] T. Hayashi, A. Yamamoto, T. Hagihara, *J. Org. Chem.* **1986**, *51*, 723–727.
- [9] E. Peña-Cabrera, P.-O. Norrby, M. Sjögren, A. Vitagliano, V. De Felice, J. Oslob, S. Ishii, D. O'Neill, B. Åkermark, P. Helquist, *J. Am. Chem. Soc.* **1996**, *118*, 4299–4313.
- [10] K. Selvakumar, M. Valentini, M. Wörle, P. S. Pregosin, A. Albinati, *Organometallics* **1999**, *18*, 1207–1215.
- [11] [11a] I. J. S. Fairlamb, G. C. Lloyd-Jones, Š. Vyskočil, P. Kočovský, *Chem. Eur. J.* **2002**, *8*, 4343–4353. [11b] L. Gouriou, G. C. Lloyd-Jones, Š. Vyskočil, P. Kočovský, *J. Organomet. Chem.* **2003**, *687*, 525–537.
- [12] J. C. Fiaud, A. Higon de Gournay, M. Larchevêque, H. B. Kagan, *J. Organomet. Chem.* **1978**, *154*, 175–185.
- [13] B. M. Trost, G. M. Schroeder, *J. Am. Chem. Soc.* **1999**, *121*, 6759–6760.
- [14] F. Ozawa, A. Kubo, Y. Matsumoto, T. Hayashi, E. Nishioka, K. Yanagi, K. Moriguchi, *Organometallics* **1993**, *12*, 4188–4196.
- [15] M. Kranenburg, P. C. J. Kamer, P. W. N. M. van Leeuwen, *Eur. J. Inorg. Chem.* **1998**, 25–27.
- [16] R. J. van Haaren, K. Goubitz, J. Fraanje, G. P. F. van Strijdonck, H. Oevering, B. Coussens, J. N. H. Reek, P. C. J. Kamer, P. W. N. M. van Leeuwen, *Inorg. Chem.* **2001**, *40*, 3363–3372.
- [17] A. C. Albéniz, P. Espinet, B. Martín-Ruiz, *Chem. Eur. J.* **2001**, *7*, 2481–2489.
- [18] M. Kollmar, B. Goldfuss, M. Reggelin, F. Rominger, G. Helmchen, *Chem. Eur. J.* **2001**, *7*, 4913–4927.
- [19] P. E. Garrou, *Chem. Rev.* **1981**, *81*, 229–266.
- [20] I. J. S. Fairlamb, G. C. Lloyd-Jones, *Chem. Commun.* **2000**, 2447–2448.
- [21] [21a] R. S. Paonessa, A. L. Prignano, W. C. Trogler, *Organometallics* **1985**, *4*, 647–657. [21b] F. Ozawa, T.-i. Son, S. Ebina, K. Osakada, A. Yamamoto, *Organometallics* **1992**, *11*, 171–176.
- [22] P. Barbaro, P. S. Pregosin, R. Salzmänn, A. Albinati, R. W. Kunz, *Organometallics* **1995**, *14*, 5160–5170.
- [23] R. J. van Haaren, H. Oevering, B. B. Coussens, G. P. F. van Strijdonck, J. N. H. Reek, P. C. J. Kamer, P. W. N. M. van Leeuwen, *Eur. J. Inorg. Chem.* **1999**, 1237–1241.
- [24] The question of an early or late transition state for this step has been a matter of debate: [24a] P. B. Mackenzie, J. Wheland, B. Bosnich, *J. Am. Chem. Soc.* **1985**, *107*, 2046–2054. [24b] J. Sprinz, M. Kiefer, G. Helmchen, M. Reggelin, G. Huttner, O. Walter, L. Zsolnai, *Tetrahedron Lett.* **1994**, *35*, 1523–1526. [24c] A. Togni, U. Burckhardt, V. Gramlich, P. S. Pregosin, R. Salzmänn, *J. Am. Chem. Soc.* **1996**, *118*, 1031–1037. [24d] B. M. Trost, L. Weber, P. E. Strege, T. J. Fullerton, T. J. Dietsche, *J. Am. Chem. Soc.* **1978**, *100*, 3416–3426. [24e] J. M. Brown, D. I. Hulmes, P. J. Guiry, *Tetrahedron* **1994**, *50*, 4493–4506. [24f] P. von Matt, G. C. Lloyd-Jones, A. B. E. Minidis, A. Pfaltz, L. Macko, M. Neuburger, M. Zehnder, H. Rügger, P. S. Pregosin, *Helv. Chim. Acta* **1995**, *78*, 265–284. [24g] P. E. Blöchl, A. Togni, *Organometallics* **1996**, *15*, 4125–4132. [24h] H. Steinhagen, M. Reggelin, G. Helmchen, *Angew. Chem. Int. Ed. Engl.* **1997**, *36*, 2108–2110. [24i] H. Hagelin, B. Åkermark, P.-O. Norrby, *Chem. Eur. J.* **1999**, *5*, 902–909.
- [25] G. C. Lloyd-Jones, S. C. Stephen, M. Murray, C. P. Butts, Š. Vyskočil, P. Kočovský, *Chem. Eur. J.* **2000**, *6*, 4348–4357.
- [26] P. R. Auburn, P. B. Mackenzie, B. Bosnich, *J. Am. Chem. Soc.* **1985**, *107*, 2033–2046.
- [27] J. C. McKew, M. J. Kurth, *J. Org. Chem.* **1993**, *58*, 4589–4595.
- [28] A. Heumann, B. Åkermark, S. Hansson, T. Rein, *Org. Synth. Coll. Vol.* **1993**, *8*, 137–140.
- [29] [29a] W. H. Bunnelle, T. A. Isbell, *J. Org. Chem.* **1992**, *57*, 729–740. [29b] B. M. Trost, M. G. Organ, G. A. O'Doherty, *J. Am. Chem. Soc.* **1995**, *117*, 9662–9670.
- [30] I. Fleming, D. Higgins, N. J. Lawrence, A. P. Thomas, *J. Chem. Soc., Perkin Trans. 1* **1992**, 3331–3349.
- [31] F. R. Hartley, S. R. Jones, *J. Organomet. Chem.* **1974**, *66*, 465–473.
- [32] B. M. Trost, P. E. Strege, L. Weber, T. J. Fullerton, T. J. Dietsche, *J. Am. Chem. Soc.* **1978**, *100*, 3407–3415.
- [33] D. G. Davis, A. Bax, *J. Mag. Res.* **1985**, *64*, 533.
- [34] P. von Matt, A. Pfaltz, *Angew. Chem. Int. Ed. Engl.* **1993**, *32*, 566–568.
- [35] P. A. Evans, J. D. Nelson, *J. Am. Chem. Soc.* **1998**, *120*, 5581–5582.
- [36] P. Sennhenn, B. Gabler, G. Helmchen, *Tetrahedron Lett.* **1994**, *35*, 8595–8598.
- [37] *OpenMoleN, Interactive Structure Solution*, Nonius B. V., Delft, The Netherlands, **1997**.
- [38] D. T. Cromer, J. T. Waber, *International Tables for X-ray Crystallography*, The Kynoch Press, Birmingham, **1974**, vol. IV, [38a] Table 2.2b, [38b] Table 2.3.1.

Received April 19, 2004

Early View Article

Published Online September 10, 2004